ARTICLE

Channels And Transporters In Immunity

Cm28, a scorpion toxin having a unique primary structure, inhibits K$_V$1.2 and K$_V$1.3 with high affinity

Muhammad Umair Naseem[1], Edson Carcamo-Noriega[2], José Beltrán-Vidal[3] (iD), Jesus Borrego[1], Tibor G. Szanto[1], Fernando Z. Zamudio[2], Gustavo Delgado-Prudencio[2] (iD), Lourival D. Possani[2], and Gyorgy Panyi[1] (iD)

The Cm28 in the venom of *Centruroides margaritatus* is a short peptide consisting of 27 amino acid residues with a mol wt of 2,820 D. Cm28 has <40% similarity with other known α-KTx from scorpions and lacks the typical functional dyad (lysine–tyrosine) required to block K$_V$ channels. However, its unique sequence contains the three disulfide-bond traits of the α-KTx scorpion toxin family. We propose that Cm28 is the first example of a new subfamily of α-KTxs, registered with the systematic number α-KTx32.1. Cm28 inhibited voltage-gated K$^+$ channels K$_V$1.2 and K$_V$1.3 with K$_d$ values of 0.96 and 1.3 nM, respectively. There was no significant shift in the conductance–voltage (G-V) relationship for any of the channels in the presence of toxin. Toxin binding kinetics showed that the association and dissociation rates are consistent with a bimolecular interaction between the peptide and the channel. Based on these, we conclude that Cm28 is not a gating modifier but rather a pore blocker. In a selectivity assay, Cm28 at 150 nM concentration (>100× K$_d$ value for K$_V$1.3) did not inhibit K$_V$1.5, K$_V$11.1, K$_{Ca}$1.1, and K$_{Ca}$3.1 K$^+$ channels; Na$_V$1.5 and Na$_V$1.4 Na$^+$ channels; or the hH$_V$1 H$^+$ channel but blocked ∼27% of the K$_V$1.1 current. In a biological functional assay, Cm28 strongly inhibited the expression of the activation markers interleukin-2 receptor and CD40 ligand in anti-CD3–activated human CD4$^+$ effector memory T lymphocytes. Cm28, due to its unique structure, may serve as a template for the generation of novel peptides targeting K$_V$1.3 in autoimmune diseases.

Introduction

Voltage-gated potassium (K$_V$) ion channels play a key role to maintain the proper physiological functions of both excitable and non-excitable cells. Pharmacological manipulation of these K$_V$ channels has a significant therapeutic prospect in the management of autoimmune diseases, cancer, and neurological and cardiovascular disorders (Coetzee et al., 1999; Cahalan and Chandy, 2009; Panyi et al., 2014; Yang and Nerbonne, 2016; Hofschröer et al., 2021). K$_V$1.3 channels are expressed in peripheral immune cells and are upregulated in effector memory T (T$_{EM}$) cells in states of autoimmunity and inflammation. Their activity maintains the electrical driving force for Ca$^+$ entry during T cell activation by the K$^+$ efflux counterbalancing the persistent Ca$^+$ influx required for proliferation and excessive release of cytokines (Cahalan and Chandy, 2009; Feske et al., 2012). Several studies have validated that specific and persistent blockade of K$_V$1.3 suppresses the T$_{EM}$ cell activation and proliferation. This dependence of T$_{EM}$ cells on K$_V$1.3 channels for proliferation brings K$_V$1.3 blockers into the spotlight as a potential therapeutic immunosuppressant to treat a range of autoimmune diseases such as multiple sclerosis, rheumatoid arthritis, type 1 diabetes mellitus, psoriasis, and others (Wulff et al., 2003; Beeton et al., 2006; Panyi et al., 2006; Toldi et al., 2010; Lam and Wulff, 2011; Serrano-Albarrás et al., 2019; Varga et al., 2021). Moreover, recent studies have demonstrated that K$_V$1.3 channels are also expressed in microglia, brain-resident macrophages, and are essential for their proliferation. Thus, K$_V$1.3 is also emerging as an attractive drug target in the treatment of neuroinflammatory disorders such as Parkinson's disease (Sarkar et al., 2020; Tajti et al., 2020; Wang et al., 2020).

[1]Department of Biophysics and Cell Biology, Faculty of Medicine, Research Center for Molecular Medicine, University of Debrecen, Debrecen, Hungary; [2]Departamento de Medicina Molecular y Bioprocesos, Instituto de Biotecnología, Universidad Nacional Autónoma de México, Cuernavaca, Mexico; [3]Grupo de Investigaciones Herpetológicas y Toxinológicas, Centro de Investigaciones Biomédicas, Departamento de Biología, Facultad de Ciencias Naturales, Exactas y de la Educación, Universidad del Cauca, Popayán, Colombia.

Correspondence to Gyorgy Panyi: panyi@med.unideb.hu

Check for updates

Several ion channel modulator peptide toxins have been identified from venomous animals such as charybdotoxin from scorpions, ShK from sea anemone, mambaquaretin-1 from snakes, and ProTx from spiders. Among the scorpion families, the Buthidae family has the most studied venoms due to its great toxicity, and several peptides reported to affect K+ channels were purified from them (Rokyta and Ward, 2017). *Centruroides margaritatus* belongs to this family and until now, only two peptides have been reported from its venom: (1) margatoxin, which blocks different K_V channels (Bartok et al., 2014), and (2) CmERG1, which completely blocks the K_V11.1 channel (Garcia-Calvo et al., 1993; Beltrán-Vidal et al., 2021). K+ channel inhibitor scorpion toxins (KTxs) have been classified into seven different families based on their structural and functional features: α-KTx, β-KTx, γ-KTx, δ-KTx, ε-KTx, κ-KTx, and λ-KTx (Tytgat et al., 1999; Rodríguez de la Vega and Possani, 2004; Tabakmakher et al., 2019). The α-KTx family contains peptides with 23–42 amino acids and share a common structural motif known as the cysteine-stabilized α/β scaffold, in which the α-helix and β-sheets are held together by 3–4 disulfide bridges. Based on the sequence similarity, 31 subfamilies of α-KTx were described previously (https://kaliumdb.org). A typical "functional dyad" consists of a critically positioned lysine residue and an aromatic residue nine positions downstream (∼6.6 Å α-carbon-benzene ring center distance in the 3-D structure), which is also considered a common characteristic of these peptides (Dauplais et al., 1997; Rodríguez de la Vega et al., 2003; Panyi et al., 2006). The critical lysine that protrudes into the selectivity filter of the channel is essential for the high-affinity block, and the aromatic residue seems responsible to determine selectivity among K_V1.x channel subtypes (Goldstein and Miller, 1993; Corzo et al., 2008; Papp et al., 2009; Bartok et al., 2015). Interestingly, there are scorpion toxins that inhibit K_V channels despite lacking the functional dyad (Batista et al., 2002; Abdel-Mottaleb et al., 2006). Moreover, for stable toxin–channel interaction, other influential residues of toxins interact pairwise with the channel residues contributing to their selectivity profile among different K_V1.x channel (Aiyar et al., 1995; Mouhat et al., 2004; Varga et al., 2021).

The ongoing discovery of K+ channel blocker peptides suggests that scorpion venoms are remarkably rich sources of these peptides. The diverse nature of their primary sequence and valuable therapeutic potential encourage the exploration of novel peptides in different scorpion venoms (Ortiz et al., 2015; Gubič et al., 2021; Varga et al., 2021). A comprehensive characterization of a Colombian scorpion *C. margaritatus* venom was reported previously by our group in order to investigate its effect on various voltage-gated K+ and Na+ channels, and a new γ-KTx (CmERG1, γ-KTx 10.1) from *C. margaritatus*, which fully blocks the human *ether-à-gogo-related* gene (hERG1) potassium channel (K_V11.1) with high affinity, was also described (Beltrán-Vidal et al., 2021). In this work, during further electrophysiological characterization of *C. margaritatus* venom components we discovered another exciting peptide, named Cm28. This peptide obeys a unique and unusual primary structure and was shown to be a potent and selective pore blocker of human K_V1.2 and K_V1.3 channels. In addition, Cm28 did not inhibit a panel of ion channels including K_V, voltage-gated sodium (Na_V), and proton (H_V) channels. Cm28 also suppressed human CD4+ effector memory T cells activation in vitro by downregulating the IL2R and CD40 ligand expression. Phylogenetic analysis conducted with the amino acid sequence of Cm28 compared with the other known K+-channel blocking peptides of scorpions, strongly support the conclusion that Cm28 is the first example of new subfamily of α-KTx blocking peptides. The uniqueness of its primary structure would provide a novel drug template for designing a highly selective K_V1.3 inhibitors.

Materials and methods

Isolation and mol wt determination of peptide toxin
A comprehensive description of venom preparation and purification approach of several peptide toxins including a short peptide Cm28 with 2,820 D mol wt from the venom of *C. margaritatus* was reported previously (Beltrán-Vidal et al., 2021). Briefly, venom was milked from scorpions by electric stimulation, dissolved in sterile water, and centrifuged at 15,000 rpm and 4°C for 15 min. The supernatant was collected, lyophilized, and stored at –20°C. To achieve high yield and purity, a three-step purification scheme was exploited. The soluble venom was first subjected to gel filtration using Sephadex G-50 column in 20 mM ammonium acetate buffer (pH 4.7) at 2 ml/min flow rate, and three fractions were collected. Fraction FII, which typically contains toxic peptides, was purified through ion-exchange chromatography (IEC) as a second step using carboxymethylcellulose column. Peptides were eluted at a flow rate of 2 ml/min with a linear gradient 0–100% of 500 mM ammonium acetate buffer over 200 min. Fractions from IEC were further purified by reverse-phase high-performance liquid chromatography (RP-HPLC) using an analytical grade C_{18} reverse-phase column (Vydac). A linear gradient from 100% of solution A (0.12% trifluoroacetic acid [TFA] in water) to 60% of solution B (0.1% TFA in acetonitrile) over 60 min was run at 1 ml/min flow rate to elute pure peptides from the column. Absorbance was monitored at 230 nm. Fractions were collected manually and stored at –20°C until further use after vacuum drying. A sample from single peaks of RP-HPLC was analyzed in LCQ Fleet mass spectrometer coupled with an electrospray ionization (Thermo Fisher Scientific, Inc.).

Peptide sequencing by Edman degradation
The primary structure of pure peptide was determined by automated Edman degradation using Biotech PPSQ-31A Protein Sequencer equipment (Shimadzu Scientific Instruments, Inc.) following the same procedure as described for another component from the same venom (Beltrán-Vidal et al., 2021). First, a pure native peptide was applied directly for sequencing, and then a reduced and alkylated sample of the same peptide was sequenced to identify cysteine residues.

Comparative analysis of peptide sequence and classification
The search for potential homologs of Cm28 was performed by BLAST using the NCBI-Non-redundant protein sequences (nr) and Uniprot Swiss-Prot databases. An additional search was

performed with the blastp option of Diamond v2.0.13.151 (Buchfink et al., 2021) against the 195 scorpion KTx sequences available in Kaliumdb (potassium channel polypeptide ligand database; Tabakmakher et al., 2019) using an e value = 1×10^{-5} as the significance cutoff. This database has >300 sequences, but here only the ones specific for K^+ channels isolated from scorpion venom were used. Identification of conserved domains was performed using Pfam (Mistry et al., 2021) and InterPro (Blum et al., 2021).

All amino acid sequence alignments were performed with mafft v7.475 (Katoh and Standley, 2013). The phylogenetic analysis by maximum likelihood was performed with iqtree v2.1.3 (Minh et al., 2020). Iterative maximum likelihood analyses were performed using all 146 α-KTx sequences of Kaliumdb to determine the group of α-KTx closest to Cm28. The sequences of the remaining families were included as outgroups. The best substitution model was determined with the modelfinder (Kalyaanamoorthy et al., 2017). Phylogenetic analysis of Cm28 was determined using the WAG + R3 model with 10,000 ultra-fast boostraps (Hoang et al., 2018). Tree was edited using FigTree1.4.4.

Modeling of Cm28
The 3-D modeling of Cm28 was performed with the help of the AlphaFold2 "colab notebook" (Mirdita et al., 2019; Jumper et al., 2021) enabling refinement with Amber-Relax (Eastman et al., 2017).

Cells
Chinese hamster ovary (CHO) cells were cultured in Dulbecco's modified Eagle's medium (DMEM, cat# 11965084; Gibco) containing 10% FBS (Sigma-Aldrich), 2 mM L-glutamine, 100 µg/ml streptomycin, and 100 U/ml penicillin-g (Sigma-Aldrich) in a humidified incubator at 37°C and 5% CO_2. Cells were passaged twice per week following a 5-min incubation in PBS containing 0.2 g EDTA/L (Invitrogen).

Human peripheral blood monocytes (PBMCs) were isolated from the venous blood of anonymous healthy donors through Histopaque1077 (Sigma-Aldrich) separation technique. PBMCs were grown (density 5×10^5 cells/ml) in RPMI 1640 medium (cat# 11875085; Gibco) supplemented with 10% FBS, 2 mM L-glutamine, 100 µg/ml streptomycin, and 100 U/ml penicillin-g in a humidified incubator at 37°C and 5% CO_2 for 3–6 d. Phyto-hemagglutinin A (PHA; Sigma-Aldrich) was also added at a concentration of 2, 5, and 10 µg/ml to activate the PBMCs and amplify the $K_V1.3$ expression. CHO cells and PBMCs were washed gently twice with 2 ml of extracellular (bath) solution (see Electrophysiology) for the patch-clamp experiments.

Heterologous expression of ion channel
CHO cells were transiently transfected using Lipofectamine 2000 kit (Invitrogen), as per manufacturer's protocol with the following ion channel coding vectors: $hK_V1.1$ (hKCNA1 gene) and $hK_V1.2$ (hKCNA2 gene) in pCMV6-AC-GFP plasmid (cat# RG211000 and RC222200; OriGene Technologies), $hK_V1.5$ in pEYFP plasmid (a kind gift from A. Felipe, University of Barcelona, Barcelona, Spain), $hK_{Ca}3.1$ (hKCNN4 gene) in pEGFP-C1

vector (a kind gift from H. Wulff, University of California, Davis, Davis, CA), $hNa_V1.5$ (hSCN5A, a kind gift from H. Abriel, University of Bern, Bern, Switzerland), and hHv1 (hVCN1, GenBank accession no. BC007277.1, a kind gift from Kenton Swartz, National Institutes of Health, Bethesda, MD). At 24 h after transfection, GFP-expressing transfectants were identified with Nikon TE 2000U fluorescence microscope using bandpass filters of 455–495 and 515–555 nm for excitation and emission, respectively, and used for current recordings (~60–70% success rate for co-transfection). In general, currents were recorded 24–36 h after transfection.

Human embryonic kidney 293 cells stably expressing $hK_V11.1$ (hERG1 and hKCNH2 genes, a kind gift from H. Wulff), $mK_{Ca}1.1$ (BK_{Ca}, mKcnma1, a kind gift from C. Beeton, Baylor College of Medicine, Houston, TX), and $hNa_V1.4$ (hSCN4A gene, a kind gift from P. Lukács, Eötvös Loránd University, Budapest, Hungary) were used.

Electrophysiology
Whole-cell currents were measured using patch-clamp technique in voltage-clamp mode following standard protocols (Hamill et al., 1981). All recordings were performed using Multiclamp 700B amplifier connected to a personnel computer with Axon Digidata1440 digitizer and Clampex 10.7 software was used for data acquisition (Molecular Devices). In general, current traces were lowpass filtered by using the built-in analog four-pole Bessel filters of the amplifiers and sampled (4–50 kHz) at least twice at the filter cutoff frequency. Micropipettes were pulled from GC150F-7.5 borosilicate capillaries (Harvard Apparatus) with tip resistance typically ranging 3–6 MΩ in the bath solution. Only those records were used for data analysis when the leak current at holding potential was <10% of peak current at the test potential. Recordings were carried out at room temperature (20–25°C). Control and test solutions were perfused into the cell through a gravity flow perfusion system. The excess bath solution was removed constantly with vacuum suction.

For the measurement of $K_V1.1$–$K_V1.3$, $K_V1.5$, $mK_{Ca}1.1$, and $Na_V1.4$–$Na_V1.5$ currents, the normal bath solution consisted of (in mM) 145 NaCl, 5 KCl, 2.5 $CaCl_2$, 1 $MgCl_2$, 5.5 glucose, and 10 HEPES, pH 7.35. To record the tail current of $K_V1.2$, the bath solution (HK-20) contained 130 mM NaCl and 20 mM KCl, and the other components remained unchanged. In the HK-150 bath, all Na^+ was substituted by K^+ to yield 150 mM K^+ concentration. In the Na^+-free extracellular solution, all Na^+ was substituted by choline-Cl, and other components remained unchanged. Equimolar substitution of Na^+ for TEA-Cl was used in the various TEA^+-containing solutions (Fig. 6). The bath solution for $K_V11.1$ consists of (in mM) 140 choline-Cl, 5 KCl, 2 $MgCl_2$, 2 $CaCl_2$, 10 HEPES, 20 glucose, 0.1 $CdCl_2$, pH 7.35; for $K_{Ca}3.1$ (in mM), 145 L-aspartic Na^+ salt, 5 KCl, 10 HEPES, 5.5 glucose, 2.5 $CaCl_2$, and 1 $MgCl_2$, pH 7.4; and for hHv1 (in mM), 60 L-aspartic acid Na^+ salt, 80 MES, 5.5 glucose, 6 $MgCl_2$, pH 7.4. The osmolarity of the extracellular solutions was between 302 and 308 mOsm/liter. All the bath solutions were supplemented with 0.1 mg/ml BSA (Sigma-Aldrich) to prevent toxin adsorption to the plastic surfaces of the perfusion system. The composition of the internal solution was (in mM) 140 KF, 2 $MgCl_2$, 1 $CaCl_2$, 10 HEPES, and

Naseem et al.
Scorpion peptide Cm28 inhibits $K_V1.2$ and $K_V1.3$

Journal of General Physiology   3 of 18
https://doi.org/10.1085/jgp.202213146

11 EGTA, pH 7.22 for recording $K_V1.1$–$K_V1.3$, $K_V1.5$, and $mK_{Ca}1.1$ currents. For $Na_V1.4$–$Na_V1.5$ currents, the internal solution consisted of (in mM) 10 NaCl, 105 CsF, 10 HEPES, and 10 EGTA, pH 7.2; and for $K_V11.1$ (in mM), 140 KCl, 2 $MgCl_2$, 10 HEPES, and 10 EGTA, pH 7.3. The internal solution for $K_{Ca}3.1$ recording contained (in mM) 150 K-Asp, 5 HEPES, 8.5 $CaCl_2$, and 1.0 $MgCl_2$, pH 7.22; and for hH_V1 (in mM), 90 L-Aspartic acid with Na, 80 MES, 6 $MgCl_2$, and 3.3 glucose, pH 6.17. The measured osmolarity of internal solutions was ~295 mOsm/liter.

All salts and positive control test chemicals for ion channel assay (ClGBI-5-chloro-2-guanidinobenzimidazole, TRAM-34, and TEA-Cl) were purchased from Sigma-Aldrich. rMgTx was in-house produced as described elsewhere (Naseem et al., 2021).

In general, for all the measurements the holding potential (V_h) was kept at –120 mV and the pulses were delivered every 15 s except when indicated. For recording the currents of $K_V1.1$–$K_V1.3$ and $K_V1.5$ ion channels, 15–300 ms long voltage pulses to +50 mV were applied. To record the $K_V1.3$ currents for conductance–voltage (G-V) relationship, activated T cells were depolarized to voltages ranging from –70 mV to +50 mV in steps of 10 mV every 15 s. For instantaneous current–voltage (I-V) relationships of $K_V1.2$ and $K_V1.3$, currents were evoked with 200-ms-long voltage ramps to +50 mV. For recording $K_V11.1$ current, voltage step to +20 mV for 1.25 s from a V_h of –80 mV followed by a step to –40 mV for 2 s was applied every 30 s, and the peak (tail) currents were recorded during the latter step. $mK_{Ca}1.1$ currents were evoked by depolarizing the cells to +100 mV for 600 ms from a V_h of –100 mV. For $K_{Ca}3.1$ currents, 150-ms-long voltage ramp to +50 mV from –120 mV was applied every 10 s. Current through the human proton channel (hH_V1) was elicited by applying a 1.0-s-long voltage ramp to +100 mV from a V_h of –60 mV every 15 s. For sodium currents through $Na_V1.4$ and $Na_V1.5$, 15-ms-long voltage steps to 0 mV were applied every 10 s.

Patch-clamp data analyses

For patch-clamp data analyses, pClamp 10.7 software package (Molecular Devices) was used. Current traces were digitally filtered with three-point boxcar filter and were corrected for ohmic leakage when needed. The inhibitory effect of a peptide toxin at a given concentration was calculated as the remaining current fraction (RCF = I / I_0, where I_0 is the peak current in the absence of the toxin, and I is the peak current at equilibrium block at a given toxin concentration). The data points (average of three to five individual records) in the dose-response curve were fitted with the Hill equation:

$$RCF = \frac{K_d^H}{K_d^H + [\text{toxin}]^H},$$

where [toxin] is the concentration of the toxin, K_d is the dissociation constant, and H is the Hill coefficient. To construct the voltage dependance of steady-state activation of $K_V1.3$, peak conductance (G) at each step voltage was calculated from peak current (I_0) at a step voltage (E_m) and K^+ reversal potential (E_K) using the chord-conductance equation $G = \frac{I_0}{(E_m - E_K)}$. Normalized conductance (G_{norm}) values were plotted as a function of voltage and points were fitted with Boltzmann sigmoidal equation:

$$G_{norm} = \frac{1}{1 + e^{\left(\frac{V_{50} - V}{k}\right)}},$$

where V_{50} is the midpoint voltage, V is the test potential, and k represents the slope factor of the function. For determination of the voltage dependence of steady-state activation of $K_V1.2$, the membrane was depolarized to different test potentials (ranging from –70 to +80 in 10 mV steps) for 300 ms, and the tail currents were recorded at –120 mV. Peak tail currents recorded following various test potentials were normalized to the maximum tail current value and plotted against the corresponding test potential. Data points were fitted with a Boltzmann sigmoidal equation as stated above.

To examine the binding kinetics, normalized peak currents (I_{norm} = I_t / I_0, where I_t is peak current in the presence of the toxin at time t and I_0 is peak current in the absence of toxin) were plotted as a function of time. Association and dissociation time constants (τ_{on}, τ_{off}) were determined by fitting the data points during the wash-in and wash-out procedures, respectively, with the single exponential function as given below:

$$I_{norm}(t) = RCF + \left[(1 - RCF) \times e^{-\frac{t}{\tau}}\right].$$

These time constants were utilized to calculate the association rate constant (k_{on}) and dissociation rate constant (k_{off}) considering a simple bimolecular interaction between the channel and the toxin, and using equations given below, also described previously in detail (Goldstein and Miller, 1993; Peter et al., 2001):

$$k_{on} = \frac{1 - (\tau_{on} \times k_{off})}{\tau_{on} \times [\text{toxin}]}, k_{off} = \frac{1}{\tau_{off}}, K_d = \frac{k_{off}}{k_{on}}.$$

Isolation of CD4+ effector memory T lymphocyte

PBMCs were isolated from a healthy donor's blood and cultured as explained earlier. Dead Cell Removal Microbead Kit (Miltenyi Biotec B.V & CO. KG) was used to eliminate the dead cells, and CD4+ T_{EM} lymphocytes were isolated through magnetic cell sorting (negative selection) with the CD4+ Effector Memory T Cell Isolation Kit (Miltenyi Biotec B.V & CO. KG). Briefly, all types of cells except CD4+ T_{EM} lymphocytes were labeled with a cocktail of monoclonal antibodies (biotin-conjugated anti-CD8, -CD14, -CD15, -CD16, -CD19, -CD34, -CD36, -CD45RA, -CD56, -CD123, -CD235a, -TCR γ/δ, and APC-conjugated anti-CCR7). Next, cells were incubated with anti-APC and anti-biotin secondary antibodies, both coupled with magnetic microbeads. The cell preparation was passed through LD Column (Miltenyi Biotec B.V & CO. KG) mounted on MidiMACS Separator (Miltenyi Biotec B.V & CO. KG), and untouched CD4+ T_{EM} lymphocytes were collected as flow through.

Activation of CD4+ T_{EM} lymphocyte

CD4+ T_{EM} lymphocytes were divided into five different treatment groups: (1) unstimulated and non-treated, (2) unstimulated and treated with Cm28 (1.5 µM), (3) stimulated only, (4) stimulated and treated with Cm28 (1.5 µM), and (5) stimulated and treated with recombinant margatoxin (rMgTx, 5 nM, produced

Naseem et al.
Scorpion peptide Cm28 inhibits $K_V1.2$ and $K_V1.3$

Journal of General Physiology   4 of 18
https://doi.org/10.1085/jgp.202213146

in-house as previously described; Naseem et al., 2021). The high concentrations of peptide toxins were used to ensure the complete blockade of $K_V1.3$ channels throughout the entire treatment duration and to counterbalance peptide adsorption to plastic surfaces and biological degradation (Beeton et al., 2011; Veytia-Bucheli et al., 2018; Naseem et al., 2021). To stimulate lymphocytes through the T cell receptor (TCR), anti-human CD3 monoclonal antibody (clone OKT3; BioLegend) was bound to the surface of a 96-well cell culture plate (cat# 3599; Corning) at 1 µg/well in PBS at 4°C overnight. Wells were washed twice with PBS to get rid of the unbound antibody. CD4+ T_{EM} cells were suspended at a density of 1×10^6 cells/ml in RPMI 1640 medium (cat# 11875085; Gibco) supplemented with 10% FBS, 2 mM L-glutamine, 100 µg/ml streptomycin, and 100 U/ml penicillin-g. To ensure the complete blockade of $K_V1.3$ prior to activation, cells were incubated with the Cm28 (at 1.5 µM) or rMgTx (at 5 nM) for 30 min. Subsequently, cells were loaded in the wells (0.2 ml of cell suspension per well) and the plate was incubated in a humidified incubator at 37°C in 5% CO_2 for 24 h. Each experiment included two technical duplicates and was performed on three different donors with the same conditions.

Flow cytometry
For assessing the cell viability, Zombie NIR fixable viability Dye (cat# 423105; BioLegend) was used. Cells were washed with PBS and incubated with Zombie NIR dye (at 1:500 dilution in 100 µl PBS) at room temperature for 20 min in dark. For staining the cells with fluorescent antibodies, cells were washed with PBS supplemented with 1% FBS and stained with PerCP/Cyanine5.5 conjugated anti-human CD25 (IL2R) antibody (clone BC96; Bio-Legend) and fluorescein isothiocyanate (FITC) conjugated anti-human CD154 (CD40L) antibody (clone 24–31; BioLegend) in 100 µl PBS + 1% FBS at 4°C for 20 min in dark. Cells were then washed with PBS + 1% FBS buffer and finally resuspended in 150 µl PBS + 1% FBS for flow cytometer analysis. Samples were measured using a NovoCyte 3000 RYB flow Cytometer (ACEA Bioscience, Inc.) and analyzed with FCS Express 6.0 (De Novo Software). Briefly, cells were gated in an FSC-H versus SSC-H density plot. Histograms corresponding to IL2R (CD25) and CD40L were generated as peak-normalized overlays. Unstained cell controls (negative) were always used for comparison, and mean fluorescent intensities were normalized to that of their stimulated but not treated control. To determine cell viability, positive staining with the Zombie NIR dye and changes in FSC were considered as indicators of dead cells. Cells treated with 30% of DMSO were used as a positive control for the viability dye.

Cytotoxicity assay
Cellular cytotoxicity mediated by peptide toxins was measured using Pierce lactate dehydrogenase (LDH) Cytotoxicity Assay Kit (Thermo Fisher Scientific) following the manufacturer's instructions. Briefly, to determine the LDH activity of a medium, 50 µl samples were obtained from the cultures following 24 h growth of the cells (stimulated or unstimulated in the presence or absence of toxin, spontaneous and maximum LDH activity

controls) and were mixed with 50 µl reaction mix (substrate) in the flat bottom 96-well plate (cat# 3599; Corning) and incubated for 30 min in dark. After adding the 50 µl of stop solution, absorbance was measured at 490 and 680 nm using Spark Multimode Microplate Reader (Tecan Trading AG). LDH activity was determined by subtracting the A_{680} (background) from the A_{490} and percentage cytotoxicity was calculated as

$$\%Cytotoxicity = \frac{\text{Toxin treat LDH activity} - \text{spontaneous LDH activity}}{\text{Maximum LDH activity} - \text{spontaneous LDH activity}} \times 100.$$

Cells treated with sterile water and lysis buffer for 45 min at 37°C were used as spontaneous and maximum LDH activity controls, respectively. For experimental positive control, cells were treated with 50 mM sodium azide (NaN_3). The experiment was repeated for three different donors.

Statistics
Statistical analyses and graph plotting were executed in GraphPad Prism software (version 8.0.1). Data were presented as mean ± SEM. For pairwise comparison, student's t test with Mann-Whitney rank sum test and for multiple comparisons, one-way ANOVA with post-hoc Tukey's test was performed. Statistical significance is indicated in terms of P values.

Online supplemental material
Fig. S1 shows the comparison of representative 3-D structures of each KTx family with the modeled 3-D structure of Cm28.

Results
Isolation and primary structure of Cm28
A detailed description about the purification of peptides from the soluble venom of C. margaritatus and their proteomic analysis was reported in our previous publication (Beltrán-Vidal et al., 2021). A three-step purification approach at the preparative level was followed to achieve a generous quantity of peptides for proteomic and functional characterization. First, soluble crude venom was fractionated into three fractions (FI, FII, and FIII) by gel filtration chromatography using Sephadex G-50 column (not shown). Then, peptide-based toxic components were separated from the main fraction FII through IEC using carboxymethylcellulose column. Finally, the 10 sub-fractions (FII.1–10, not sown) from IEC were individually subjected to reverse-phase HPLC. A peptide with mol wt 2,820.5 D was discovered in HPLC fraction of FII.6 (Fig. 1 A) in addition to another novel peptide blocker (CmERG1, γ-KTx 10.1) of $K_V11.1$ (hERG1) channel (Beltrán-Vidal et al., 2021). The 2,820.5 D peptide was called "Cm28," corresponding to the scorpion's name C. margaritatus and its mol wt. Cm28 peptide was eluted at 24.5 min retention time from C_{18} HPLC column as indicated in Fig. 1 A. The full-length amino acid sequence of Cm28 was determined by direct automatic Edman degradation of native peptide and, alkylated and reduced forms of peptide. This novel peptide contains 27 amino acids with 6 cysteines and 3 potential disulfide bridges (Fig. 1 B). The primary structure of Cm28 is unique and unusual because it has fewer residues and is a completely
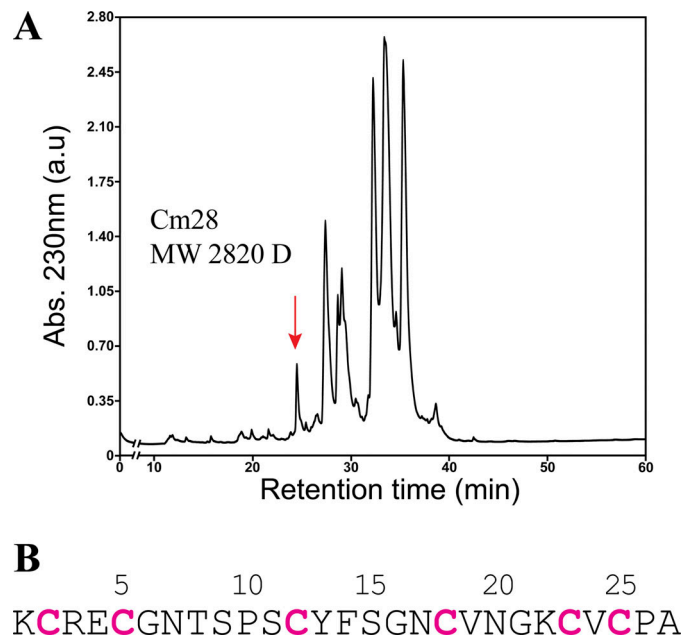
Naseem et al.
Scorpion peptide Cm28 inhibits $K_V1.2$ and $K_V1.3$

Journal of General Physiology   5 of 18
https://doi.org/10.1085/jgp.202213146

A

B

```
        5         10        15        20        25
KCRECGNTSPSCYFSGNCVNGKCVCPA
```

Figure 1. **Isolation of Cm28 peptide from the venom of *C. margaritatus* and primary sequence determination. (A)** Final step reverse-phase HPLC separation of venom components from fraction FII.6 (see Results for details). A linear gradient of 0–60% acetonitrile over 60 min was run to elute the peptides. Cm28 peptide was eluted at a retention time of 24.5 min, indicated with a red arrow. **(B)** Full-length primary structure of Cm28 was acquired by automatic Edman degradation using the conditions described in Materials and methods. Cysteine residues are highlighted in magenta. MW, molecular weight.

different sequence than other known scorpion toxins blocking K$^+$ channels.

Sequence and phylogenetic analysis of Cm28

No homologous amino acid sequences of Cm28 were identified by BLAST in the NCBI and UniProt databases. However, diamond blastp analysis against kaliumdb sequences revealed α-KTx13.4 (*Tityus stigmurus*, UniProt accession no. P0C8L2), ε-KTx1.2 (*Titus serrulatus*, UniProt accession no. P0C175) and ε-KTx1.1 (*T. serrulatus*, UniProt accession no. P0C174) as potential homologs of Cm28. Alignment of the representative sequences shows that their percent identity ranges from 23 to 42% (Fig. 2), with the C-terminal region of the peptides being the most conserved. No Pfam domain was identified in Cm28 as reported by http://pfam.xfam.org/ (Mistry et al., 2021). Phylogenetic analysis was performed by comparing the amino acid sequence of Cm28 with 75 other reported scorpion toxins (Kaliumdb/UnitProt; Fig. 3). Cm28, ε-KTx1.1, and ε-KTx1.2 toxins clustered within the α-KTx family suggest that these three toxins belong to this KTx family. Moreover, the 3-D structure of Cm28 (Fig. S1) shows one short α-helix connected to an antiparallel β-sheet stabilized by three disulfide bonds (CSα/β), a similar motif found in the structure of the α-KTx toxins.

Cm28 inhibits human K$_V$1.2 and K$_V$1.3 with low-nanomolar affinity

The primary structural features make Cm28 an exceptional scorpion toxin; therefore, we assessed if such an unusual peptide has any pharmacological activity against K$^+$ channels. First, we aimed at testing the effects of Cm28 on two human K$^+$ channels, K$_V$1.2 and K$_V$1.3. The macroscopic K$_V$1.2 currents were measured

in transiently transfected CHO cells (see Materials and methods for detail). Channels were activated by a series of depolarization pulses to +50 mV from –120 mV. Due to the highly variable activation kinetics of K$_V$1.2 (Rezazadeh et al., 2007), 15–500-ms long pulses every 15 s were applied to maximize the open probability of the channel. The slower inactivation rate of K$_V$1.2 prevented inactivation even at 500-ms-long depolarization pulses. For K$_V$1.3 current measurements, human peripheral T lymphocytes were activated by Phytohemagglutinin A (PHA) to boost up the expression of K$_V$1.3 channels, and the pipette-filling solution was Ca^{2+} free to avoid K$_{Ca}$3.1 channel activation. Thus, the whole-cell currents were recorded exclusively through K$_V$1.3 channels, as shown previously (Gurrola et al., 2012; Varga et al., 2012). The K$_V$1.3 currents were evoked by 15-ms-long depolarization pulses to +50 mV. The use of short pulses every 15 s ensured that there is no cumulative inactivation of K$_V$1.3 channel. Cm28 dissolved freshly in the extracellular solution was applied through a custom-built micro perfusion system at the rate of 200 µl/min. The complete exchange of solution in the bath chamber, i.e., the proper operation of the perfusion apparatus, was confirmed frequently using fully reversible inhibitors as positive controls at a concentration equivalent to their K$_d$ values (i.e., 14 nM charybdotoxin [ChTx] for K$_V$1.2 [Fig. 4 A] and 10 mM TEA$^+$ for K$_V$1.3 [Fig. 4 B]), and the ~50% inhibition in peak current was an indicator of both the ion channel and the proper operation of the perfusion system.

Fig. 4 A represents the whole-cell currents through K$_V$1.2 recorded sequentially in the same cell, before (control trace, black) and after perfusing the cell with 2 nM Cm28 till the equilibrium block (purple trace). At equilibrium block, Cm28 showed ~70% reduction in current amplitude. The block was

```
                        10        20        30        40    len   %ID
              ....|....|....|....|....|....|....|....|..
Cm28          -----KCRECGN--TSPSC------YFSGNCVNGKCVCPA--    27   100
ε-KTx_1.1|T. serrulatus|P0C174   ---KP..GL.RYRCC.GG.-------S..K.....A.D.S---   29   42
ε-KTx_1.2|T. serrulatus|P0C175   ---TV..GG.NRKCC.AGG.-------R..K.I....Q.Y*--   30   39

α-KTx_13.4|T. stigmurus|P0C8L2   --------G.RQ--CGGG.------NKH.K.I....K.Y*--   24   33
α-KTx_13.1|T. obscurus|P83243    -----A.GS.RKK-CKG----------..K.I.R.K.Y---    23   32
α-KTx_13.3|T. pachyurus|P84630   -----A.GS.RKK-CKG----------P.K.I.R.K.Y*--    24   29
α-KTx_23.2|V. mexicanus|P0DJ32   -AAAIS.VGSKE--CL.K.KA--QGCK..K.M.K..K.YC--   35   29
α-KTx_2.1|C. noxius|P08815       TIINV..TSPKQ--C.KP.KELYGSSAGAK.M....K.YNN*   40   25
α-KTx_2.8|C. elegans|P0C161      TVINV..TSPKQ--CLKP.KDLYGPHAGAK.M....K.YNN-   39   23
```

Figure 2. **Multiple alignment of Cm28 with other representative KTx.** Len, mature chain length; %ID, percent amino acid identity. Conserved cysteine residues are highlighted in yellow. Identical positions to those in Cm28 are indicated by dots, and * indicates that the C-terminal is amidated.

almost fully reversible upon washing the perfusion chamber with toxin-free solution (wash-out trace, green in Fig. 4 A). The onset and recovery from the block of $K_V1.2$ currents at 2 nM Cm28 are shown in Fig. 4 C. Normalized peak currents were plotted as a function of time. Both the association and dissociation processes of Cm28 were very slow and, accordingly, the development of equilibrium block and recovery up to ~85% of control current took several minutes. Similar sets of experiments were carried out for $K_V1.3$: 2 nM Cm28 inhibited ~58% of the $K_V1.3$ current upon reaching the block equilibrium. Fig. 4 B displays the current traces recorded sequentially in the same T lymphocyte, in the presence (red trace) and absence (black trace) of Cm28 peptide. Like $K_V1.2$, the block of $K_V1.3$ was also reversible (90% recovery took 10 min) upon perfusing the cell with toxin-free solution (wash-out trace, green in Fig. 4 B). The onset of steady-state block and relief from the block took comparatively less time than for $K_V1.2$ as shown in Fig. 4 D, indicating that the association and dissociation steps are faster for $K_V1.3$ than $K_V1.2$.

We performed a concentration–response experiment to determine the concentration-dependent block of $K_V1.2$ and $K_V1.3$ channels by Cm28. Different concentrations of Cm28 were applied to the cell for an adequate duration to reach the complete equilibrium block, considering the slow blocking kinetics, especially at low toxin concentrations. The remaining current fractions were calculated as (I/I_0, where I_0 is the peak current in the absence of the toxin and I is the peak current at equilibrium block in the presence of Cm28 at a given concentration). Data points were fitted with Hill equation (see Materials and methods for details) to obtain dose–response curves. The resulting dissociation constant (K_d) values and Hill coefficients (H) were K_d = 0.96 nM, H = 1.04 for $K_V1.2$ (Fig. 4 E) and K_d = 1.3 nM, H = 0.93 for $K_V1.3$ (Fig. 4 F). Cm28 showed a similar affinity for both channels.

Mechanism of block

Traditionally, most of the known toxins inhibit the K_V channels by following two modes of action. First, simple pore blocking in which toxins physically occlude the pore region preventing the permeation of K+ ions. In the second mechanism, toxins bind to

the voltage-sensing domain of the K_V channels and modulate its gating by causing a prominent shift in the voltage dependence of steady-state activation toward more depolarized potentials and consequently, reduce the K+ current (Swartz and MacKinnon, 1997; Moreels et al., 2017). The blocking mechanism of Cm28 was assessed by determining the voltage dependence of steady-state-activation and the threshold voltage of activation for both $K_V1.2$ and $K_V1.3$ ion channels. Instantaneous I-V relationship was recorded using CHO cells for $K_V1.2$ and activated T cells for $K_V1.3$ (Fig. 5, A and B). Currents were evoked by applying 200-ms-long voltage ramps from –120 mV to +50 mV every 15 s. Cm28 did not shift the threshold voltage of activation of either current as shown in Fig. 5, A and B. The current traces in the control solution and at the equilibrium block with 2 nM Cm28 showed a similar threshold voltage of activation; approximately –23 mV for $K_V1.2$ (Fig. 5 A) and approximately –40 mV for $K_V1.3$ (Fig. 5 B).

For the construction of G-V relationship for $K_V1.2$, isochronal tail peak currents were recorded in CHO cells at –120 mV followed by 300-ms long depolarizations ranging from –70 to +80 in 10 mV steps from V_h –120 mV in HK-bath containing 20 mM K+ to increase the tail currents. Due to highly variable activation properties (Rezazadeh et al., 2007), only those records were considered for analysis that had a similar gating mode. Normalized tail peak currents were plotted as a function of membrane potential (E_m) in Fig. 5 C, the solid lines represent the best-fit Boltzmann sigmoidal function. Cm28 did not introduce any substantial shift in the G-V curve of $K_V1.2$ (Fig. 5 C). The midpoint voltage (V_{50}) of the G-V relationship for $K_V1.2$ was 21 ± 3 mV in the control solution (n = 5) and 15 ± 4 mV at equilibrium block with 2 nM Cm28 (n = 5). Fig. 5 E indicates that the difference between V_{50} for $K_V1.2$ in the presence or absence of Cm28 was statistically nonsignificant. For G-V relationship of $K_V1.3$, whole-cell currents in the activated human T lymphocytes were measured in response to voltage pulses ranging from –70 to +50 mV in 10 mV steps from V_h of –120 mV, and the conductance values were calculated for each test potential and normalized for the maximal conductance. The best fit of the Boltzmann sigmoidal function to the averaged data points yielded the superimposed solid lines as shown in Fig. 5 D, indicating that there is no change in the voltage dependence of steady-state
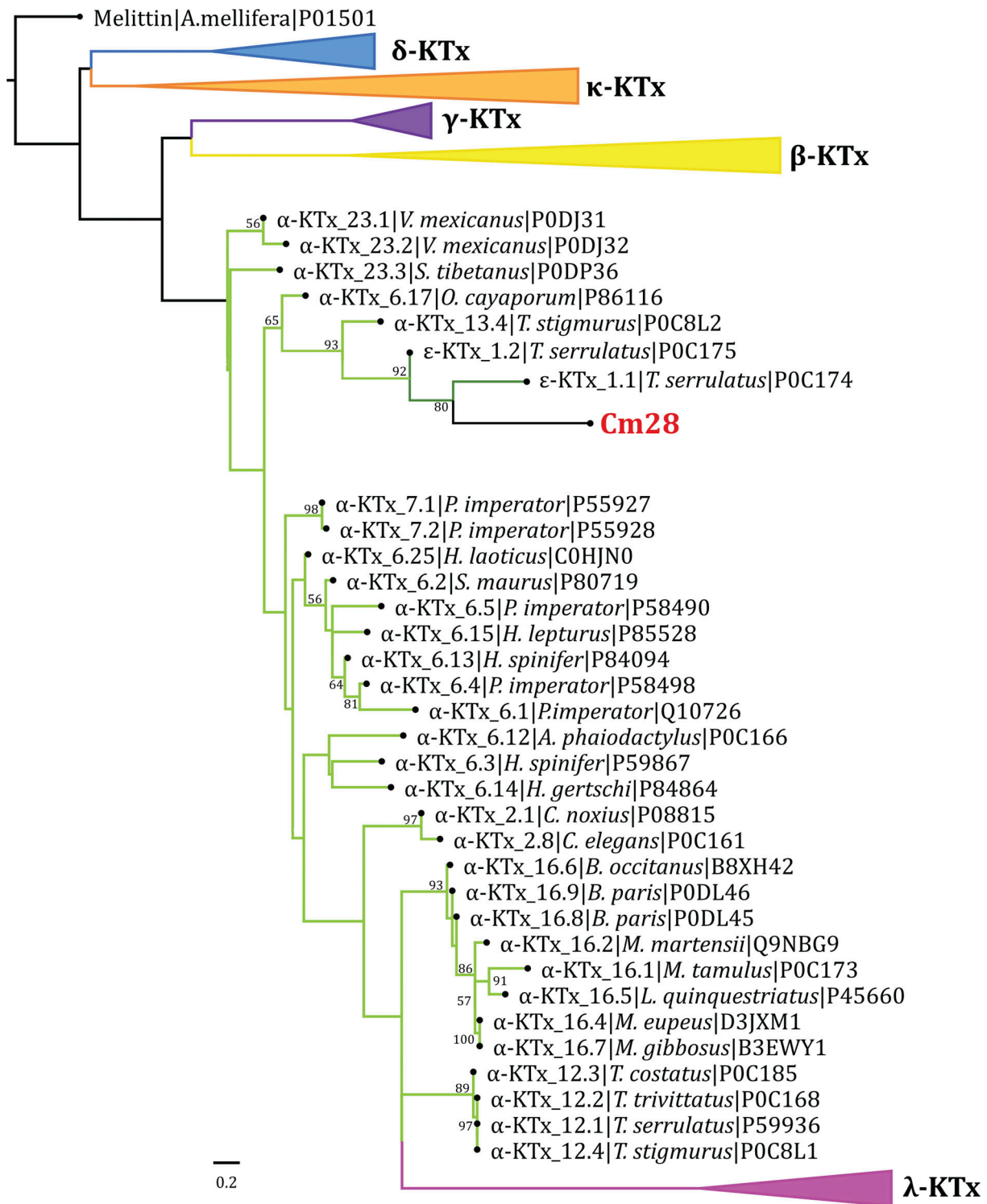
Figure 3. **Phylogenetic analysis of Cm28.** Maximum likelihood tree topology obtained from the analysis of Cm28 and other related KTxs (Log-likelihood = −4445.324618). The numbers below the nodes indicate bootstrap support values (UFBoot) >50.

activation of $K_V1.3$ in the presence of Cm28 at 2 nM, similar to $K_V1.2$. The V_{50} values for $K_V1.3$ were similar in the control solution (V_{50} = −20 ± 3, n = 4) and at an equilibrium block with 2 nM Cm28 (V_{50} = −19 ± 2, n = 4) as shown in Fig. 5 E. As the voltage dependence of steady-state activation and the threshold voltage of activation were not affected by the Cm28 for both

$K_V1.2$ and $K_V1.3$ ion channels, it suggests that Cm28 is not a gating modifier, rather that it interacts with the pore region of ion channels.

Fig. 5 F displays the analysis of kinetic parameters of the development of $K_V1.3$ current inhibition at different Cm28 concentrations. The time constant for the development of the
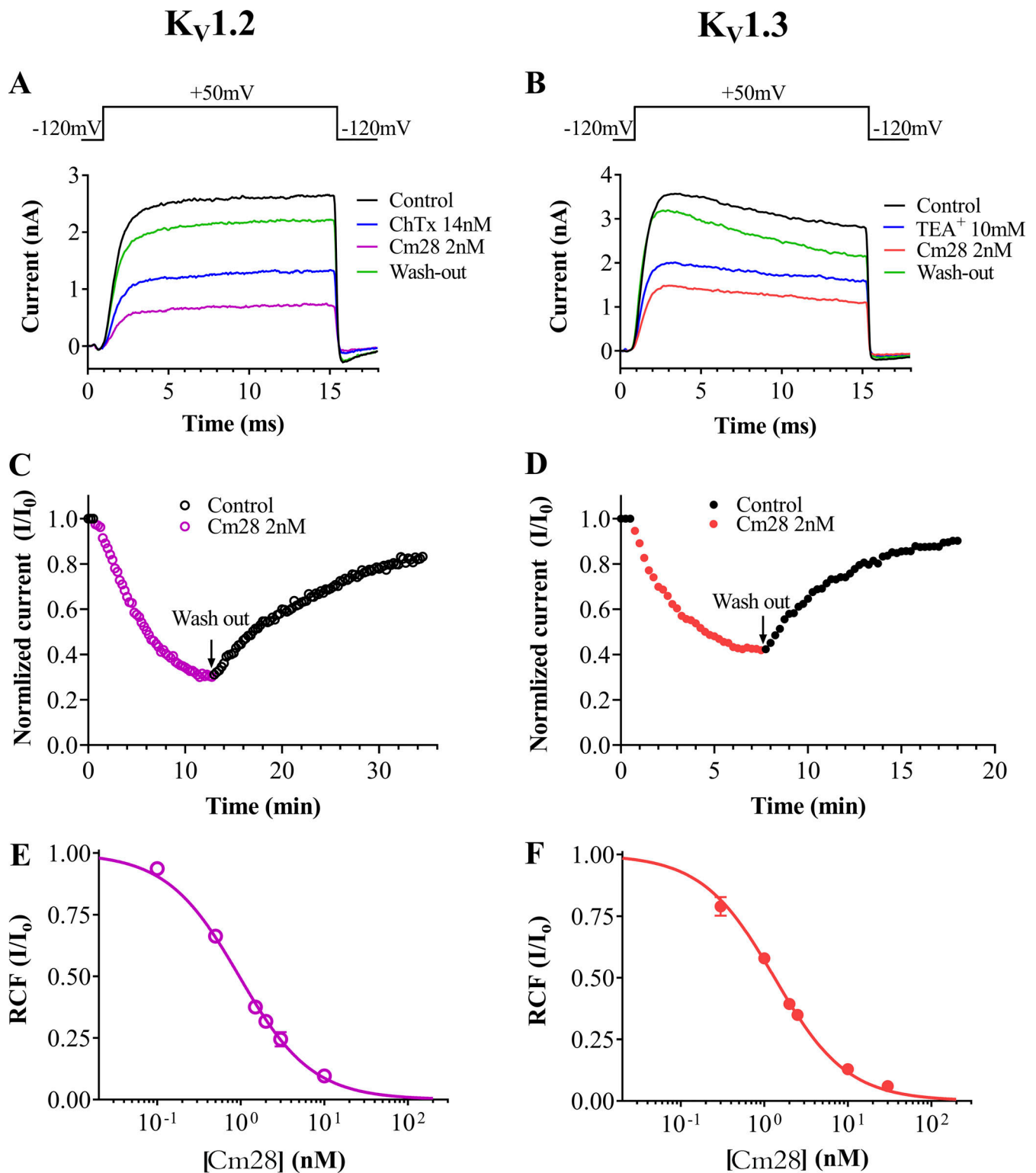
Figure 4.   **Inhibition of K_V1.2 and K_V1.3 currents by Cm28. (A and B).** Whole-cell currents of K_V1.2 (A) and K_V1.3 (B) were recorded on transiently transfected CHO cells and activated human peripheral T lymphocytes, respectively, by applying 15-ms-long voltage pulses to +50 mV from a V_h of −120 mV every 15 s. Representative current traces show the K^+ current in control solution (black), at equilibrium block in the presence of 14 nM ChTx for K_V1.2, and 10 mM TEA^+ for K_V1.3, (blue traces in A and B, respectively) as a perfusion control, at equilibrium block upon application of 2 nM Cm28 (purple for K_V1.2, red for K_V1.3) and after recovery from the block upon application of toxin-free solution (green, wash-out). **(C and D)** Time course of development and recovery of the K^+ current inhibition. Normalized peak currents were plotted as function of time. Data points in purple (C, K_V1.2) and in red (D, K_V1.3) represent the application of 2 nM of Cm28 to the bath solution. Upon reaching the block equilibrium, cells were perfused with toxin-free solution (arrow, wash out) to demonstrate reversibility of the block (data points in black). **(E and F)** Concentration-dependent block of K_V1.2 (E) and K_V1.3 (F) by Cm28. A Hill equation (see Materials and methods for details) was fitted to the RCF values calculated at different toxin concentrations (solid lines). The best fit resulted in K_d = 0.96 nM, H = 1.04 for K_V1.2 (E) and K_d = 1.3 nM, H = 0.93 for K_V1.3 (F). Error bar represents SEM and n = 3–5.
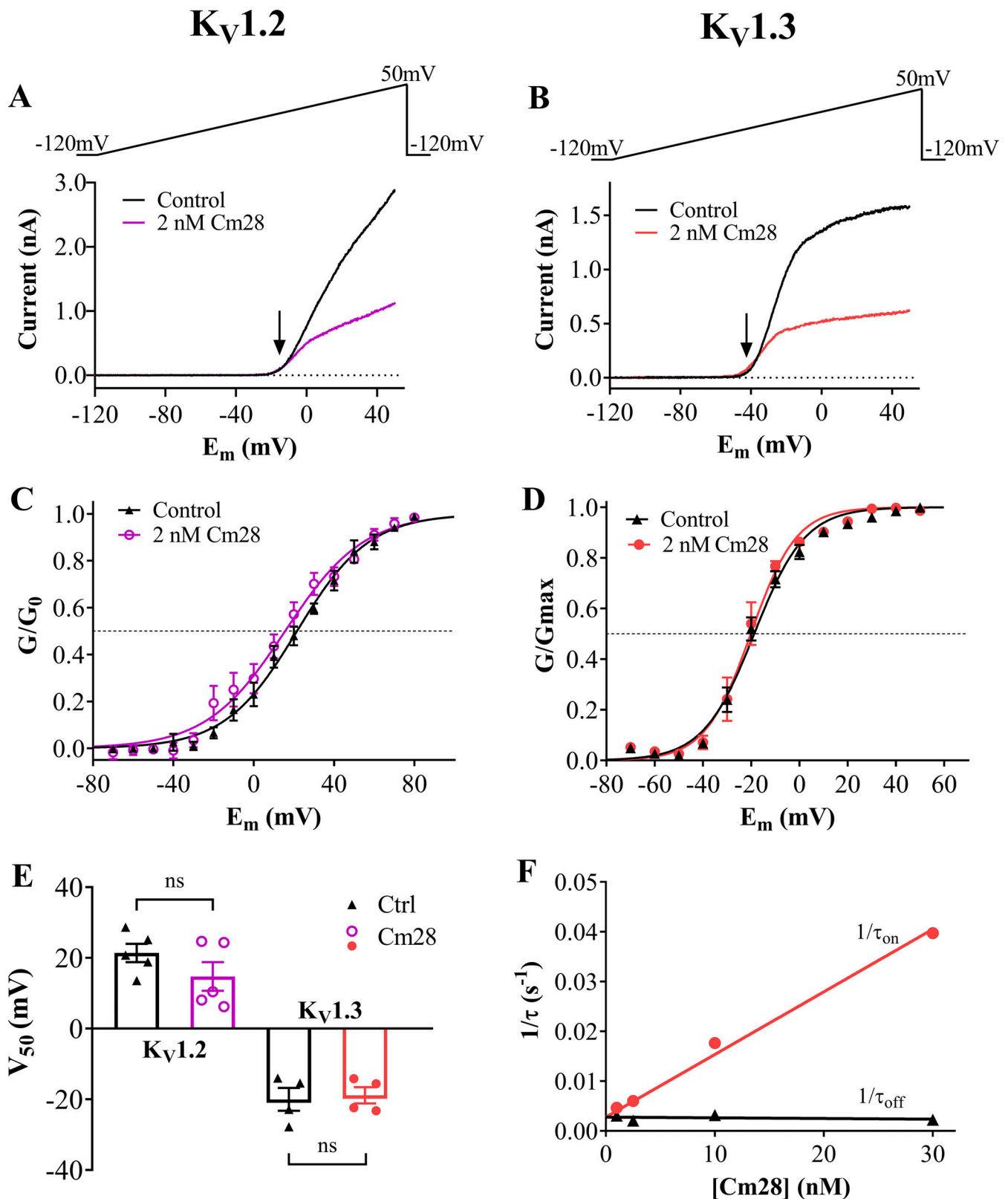
K$_V$1.2

K$_V$1.3

Figure 5. **Mechanism of blocking K$_V$1.2 and K$_V$1.3 by Cm28. (A and B)** Instantaneous I-V relationship for K$_V$1.2 (A) and K$_V$1.3 (B). Cells were held at −120 mV and depolarized to +50 mV in 200 ms using a voltage ramp protocol (at a rate of 0.85 mV/ms). Test pulses were applied every 15 s. Representative traces show the average of three traces either in the control solution (black) or at equilibrium block in the presence of 2 nM Cm28 (purple for K$_V$1.2 in A and red for K$_V$1.3 in B). Arrows indicate the activation threshold voltages. **(C and D)** G-V curve for K$_V$1.2 (C) was constructed from isochronal tail current amplitudes recorded in CHO cells at −120 mV. The currents were activated by 300-ms-long depolarizing test potentials ranging from −70 to +80 mV in 10 mV increments from a V$_h$ of −120 mV. Tail currents were normalized to maximum and plotted as a function of membrane protentional (E$_m$). To obtain the G-V curve of K$_V$1.3 (D), whole-cell

currents were measured in activated human T lymphocytes by applying voltage pulses ranging from –70 to +50 mV in 10 mV steps from V_h of –120 mV. Then, normalized conductance was calculated using the chord-conductance equation (see Materials and methods) and plotted against membrane potential (E_m). The Boltzmann sigmoidal equation was fitted to the averaged data points (solid lines). The voltage dependence of steady-state activation curve was determined in the absence (filled up triangles in black) or in the presence (empty circles in purple for $K_V1.2$ and filled circles in red for $K_V1.3$) of 2 nM Cm28. **(E)** V_{50} values from G-V curves of individual cells were averaged and plotted as bar graphs. Symbols indicate individual data points obtained in the absence (triangles) or in the presence (empty circles in purple for $K_V1.2$ and filled circles in red for $K_V1.3$) of 2 nM Cm28. Mann–Whitney test, $P = 0.23$ ($K_V1.2$) and $P = 0.57$ ($K_V1.3$). **(F)** Effect of Cm28 concentrations on the binding kinetics to $K_V1.3$. The $1/\tau_{on}$ values, (circles) and dissociation rate constant ($1/\tau_{off}$ or k_{off}, triangles) were plotted as a function of Cm28 concentrations. Data points were fitted with linear regression ($r^2 = 0.99$). Error bars in C–F represent SEM and $n \geq 3$.

block (τ_{on}, association or wash-in time constant) was obtained by fitting a single-exponential decay function to the normalized peak currents in the presence of Cm28 (Fig. 4 D). The time constant for the recovery from block (τ_{off}, dissociation or wash-out time constant) was determined by fitting a single exponential rising function to the normalized peak currents during the wash-out procedure (Fig. 4 D). With the assumption of a simple bimolecular reaction between the toxin and the channel, the resulting wash-in and wash-out time constants can be expressed as follows:

$$\tau_{on} = \frac{1}{k_{on} \times [Cm28] + k_{off}}, \tau_{off} = \frac{1}{k_{off}},$$

where k_{on} is the second-order association rate constant, k_{off} is the first-order dissociation rate constant, and [Cm28] is the toxin concentration. Plotting the $1/\tau_{on}$ and dissociation rate constant ($1/\tau_{off}$ or k_{off}) values as a function of the Cm28 concentrations showed that the $1/\tau_{on}$ increases linearly with toxin concentration, whereas the dissociation rate remains constant with $k_{off} = 0.0028 \pm 2.15 \times 10^{-4}$ s^{-1}, similar to ChTx binding to Shaker as described previously (Goldstein and Miller, 1993). The slope of superimposed regression line fitted to the $1/\tau_{on}$ data points, using 0.0028 s^{-1} as the y intercept, corresponds to second-order rate constant of association with $k_{on} = 0.0013 \pm 2.6 \times 10^{-5}$ nM^{-1} s^{-1} ($r^2 = 0.99$; Table 1).

Similarly, the association (τ_{on}) and dissociation (τ_{off}) time constants of $K_V1.2$ blockade at 2 nM Cm28 were determined by fitting the single exponential function to data points during the wash-in procedure and wash-out procedure (Fig. 4 C). Like $K_V1.3$, assuming the bimolecular interaction between the toxin and the channel k_{on} and k_{off} rate constant were

calculated using the above-mentioned equations and time constants (Table 1).

The dissociation constants ($K_d = k_{off}/k_{on}$) calculated from the block kinetics yielded 1.18 nM for $K_V1.2$ and 2.15 nM for $K_V1.3$, as given in Table 1, that are in good agreement with the K_d values obtained from equilibrium block (Fig. 4, E and F).

Selectivity profile of Cm28

To reveal the selectivity profile of Cm28, we assayed the effect of Cm28 on two members of voltage-gated *Shaker* family channels, h$K_V1.1$ (Fig. 6 A) and h$K_V1.5$ (Fig. 6 B), that are closely related to the channels inhibited by Cm28. In addition, we also tested the effect of Cm28 on h$K_V11.1$ (hERG1, Fig. 6 C), a voltage-gated cardiac K$^+$ channel; h$K_{Ca}3.1$ (IKCa1, SK4, Fig. 6 D), the Ca^{2+} activated K$^+$ channel expressed in T lymphocytes; m$K_{Ca}1.1$ (BK, Slo1, MaxiK, Fig. 6 E), the large conductance voltage- and Ca^{2+}-activated channel; two voltage-gated sodium channels, h$Na_V1.4$ (Fig. 6 F) and h$Na_V1.5$ (Fig. 6 G), expressed in skeletal and cardiac muscles, respectively; and hH_V1 (Fig. 6 H), a voltage-gated proton channel. We found that, except $K_V1.1$, none of the ion channels tested (Fig. 6, A–I) were inhibited by Cm28 at 150 nM concentration, which is >150-fold concentration than the K_d for $K_V1.2$ and >100-fold than the K_d for $K_V1.3$. The application of 150 nM Cm28 reduced ~27% of $K_V1.1$ current and the RCF value was 0.73 ± 0.03 ($n = 3$). The estimated K_d value for $K_V1.1$ from a single concentration, based on a bimolecular interaction, yielded ~0.4 μM. The amount of native peptide was not sufficient to construct a complete dose-response curve at this very high peptide concentration range.

Cm28 peptide does not compromise cell viability but suppresses the expression of activation markers in CD4$^+$ T$_{EM}$ cells

After characterizing the pharmacological properties of the unique Cm28 peptide with electrophysiology, we investigated whether these features reflect in biological functional assays. As the main aim of this assay was to evaluate the effect of Cm28 on the TCR-mediated activation of CD4$^+$ T$_{EM}$ cells, first we had to determine whether the peptide compromises cell viability. Following a 24-h culture period in the presence of 1.5 μM Cm28 or 50 nM rMgTx, the viability of CD4$^+$ T$_{EM}$ cells was not impaired either in quiescent or TCR-activated cells as analyzed by two different assays (Fig. 7). Staining the cells with a fixable viability dye Zombie NIR followed by flow cytometry identified that ≥90% of cells were viable in the presence of either toxin. 30% DMSO was added to the cells for 30 min as a positive control for dead cells (Fig. 7 A). In parallel, the LDH activity assay revealed that cytotoxicity of Cm28 was <1% and that of rMgTx was <2% for either quiescent or

Table 1. Kinetic parameters for binding of Cm28 to $K_V1.2$ and $K_V1.3$ channels

	Mean ± SEM	
	$K_V1.2$	$K_V1.3$
k_{on} (nM^{-1} s^{-1})	0.0011 ± 7.17 × 10^{-5}	0.0013 ± 2.63 × 10^{-5}
k_{off} (s^{-1})	0.0013 ± 2.94 × 10^{-5}	0.0028 ± 2.15 × 10^{-4}
K_d (nM)	1.18 ± 0.047	2.15 ± 0.12
n	4	4

For $K_V1.2$, the k_{on} and k_{off} were calculated from time constants (τ_{on}, τ_{off}) for the onset and recovery of the block in the presence of 2 nM Cm28. For $K_V1.3$, k_{on} and k_{off} were determined by the fitting the $1/\tau_{on}$ and $1/\tau_{off}$ values with linear regression function (Fig. 5 F, see Results for details). K_d was determined as k_{off}/k_{on}.
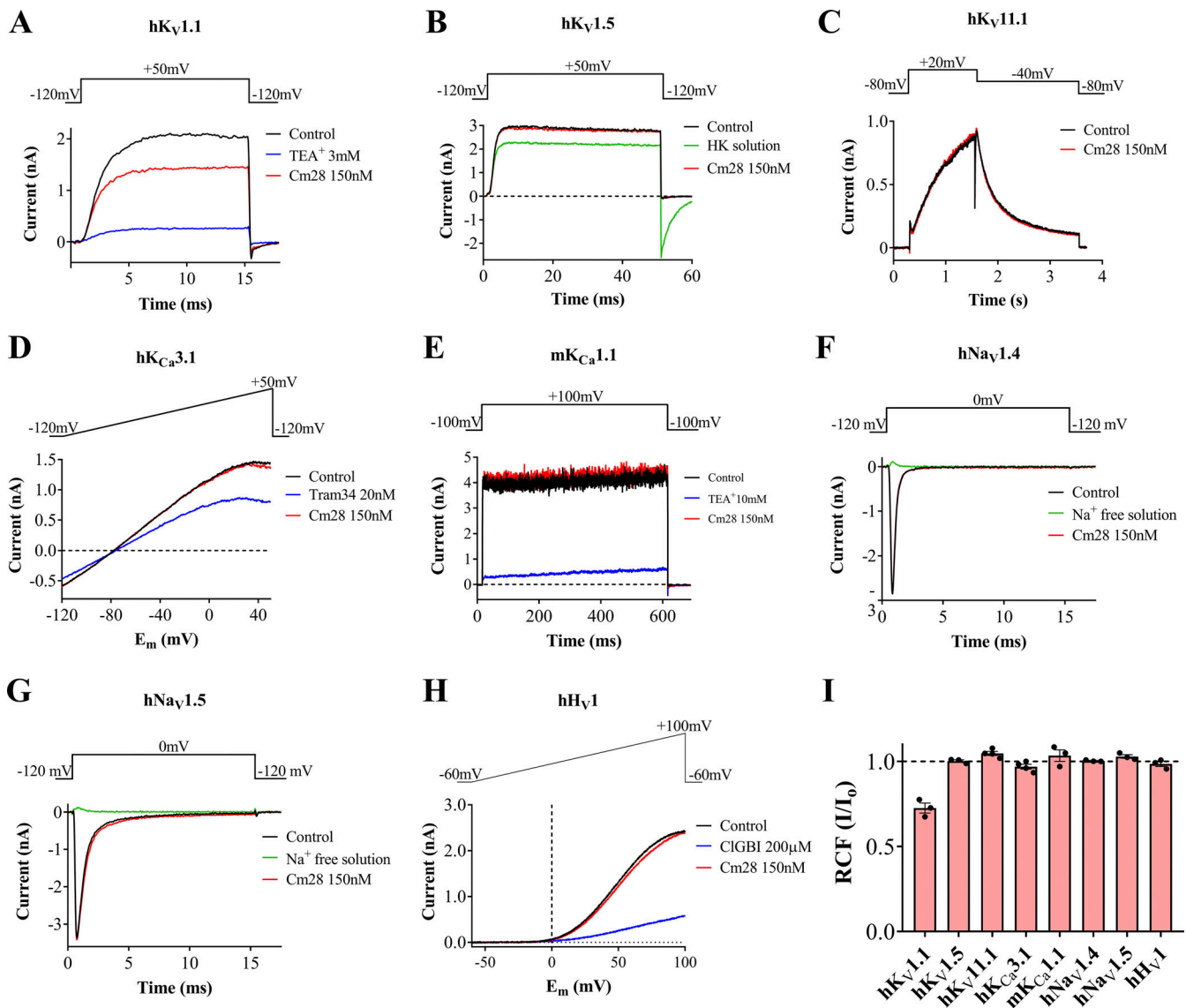
Figure 6. **Selectivity profile of Cm28. (A–H)** Representative current traces are shown in the absence of (indicated as control in black) and presence of 150 nM Cm28 (>100× of K_d value for $K_V1.3$) of Cm28 (in red). The proper operation of solution exchange in a recording chamber was tested frequently using fully reversible blockers (shown in blue) or solutions (in green) as a positive control (HK: HK-150 solution with 150 mM extracellular K^+ to reduce the K^+ driving force or TEA^+, Tram34, and ClGBI are known blockers of appropriate channels). Voltage protocols are shown above the current records in each panel. For external and internal solution composition, see Materials and methods. The traces shown in the presence of 150 nM Cm28 were recorded at equilibrium block (A) or after 8–20 pulses (2–5 min) in the presence of Cm28 (B–H). **(I)** Remaining current fractions for the indicated channels. Normalized RCF (I/I_0) values were calculated as the ratio of the peak currents in the presence (I) or absence (I_0) of 150 nM Cm28 at equilibrium block (for $K_V1.1$) or after 8–20 repeated depolarization pulse. Bars and error bars indicate the mean ± SEM ($n \geq 3$).

TCR-activated T_{EM} cells after 24 h culture period. 50 mM NaN_3, as the positive control, showed 15% cytotoxicity (Fig. 7 B).

In human T lymphocytes, the expression of the Ca^{2+}-dependent early activation markers in the cell membrane, such as IL2R and CD40 ligand, is upregulated upon TCR-mediated activation. These activation markers have been used as a readout to assess $K_V1.3$-dependence of T cell activation (Balajthy et al., 2016; Veytia-Bucheli et al., 2018; Naseem et al., 2021). $CD4^+$ T_{EM} cells were pre-incubated for 30 min with either 1.5 μM Cm28 (>1,000× concentration of its K_d for $K_V1.3$) or 5 nM rMgTx (100× concentration of its K_d for $K_V1.3$, as positive control), and the cells were then activated for 24 h with plate-bound anti-human

CD3 antibody in the continuous presence of toxins. The flow cytometric overlayed histograms in Fig. 8, A and C show that Cm28 (red traces) significantly reduced the fraction of CD40L (Fig. 8 A) and IL2R (Fig. 8 C) expressing T_{EM} cells, similar to rMgTx (blue trace), as compared with the control cells stimulated identically in the absence of toxin (green trace). The expression of CD40L (Fig. 8 B) and IL2R (Fig. 8 D) in Cm28-treated T cells, normalized to that of stimulated but not treated cells, is reduced to ∼47 and ∼55%, respectively. Similarly, positive control rMgTx decreased the CD40L and IL2R expression levels to ∼51 and ∼48%, respectively. There was no change in the expression of CD40L or IL2R in $CD4^+$ in T_{EM} cells not exposed to
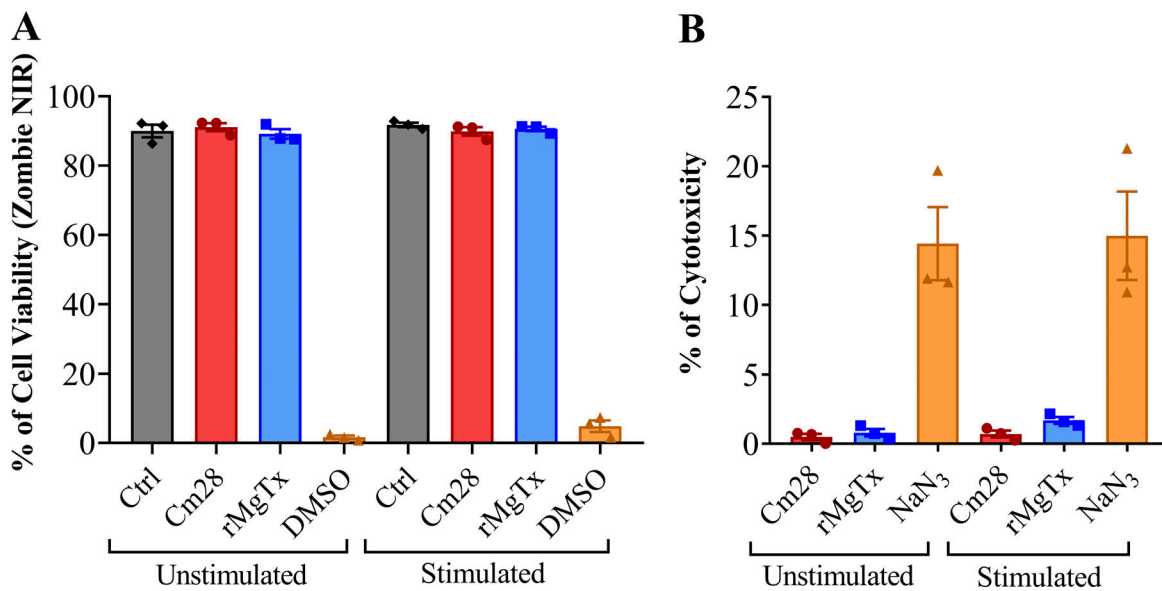
Figure 7. **Cm28 does not compromise the cell viability of either quiescent or stimulated CD4$^+$ T$_{EM}$ lymphocytes. (A)** Cell viability in the presence of 1.5 μM Cm28 or 50 nM rMgTx was assessed by staining the cells with fixable viability dye Zombie NIR after 24 h culture period using flow cytometry. Changes in FSC and positive staining with the Zombie NIR were considered indicators of dead cells (see Materials and methods). The percentage of cell viability was calculated as: 1—fraction of Zombie NIR positive cells. Cells were treated with 30% DMSO for 30 min before staining as a positive control for dead cells. Control cells (Ctrl) were not exposed to peptides. **(B)** The cytotoxic effect of 1.5 μM Cm28 or 50 nM rMgTx on T$_{EM}$ cells determined using the LDH cytotoxicity assay. LDH activity of the medium was determined following 24 h culture period and percentage of cytotoxicity was calculated (see Materials and methods for details). For positive control, 50 mM NaN$_3$ was added to the cells. **(A and B)** Data from three independent experiments (two technical repeats in each) are shown as mean ± SEM.

anti-CD3 antibody regardless of the presence (US + Cm28) or absence of Cm28 (US; Fig. 8).

Discussion

In this article, we characterized the in vitro pharmacological and immunological activities of Cm28, a novel peptide isolated from *C. margaritatus* belonging to the Buthidae family of scorpions. Cm28 consists of only 27 amino acids with 6 cysteine residues. It is a high-affinity blocker of human K$_V$1.2 and K$_V$1.3 channels with K$_d$ values of 0.96 and 1.3 nM, respectively. It also inhibited K$_V$1.1 channel with low affinity. The application of high concentration (~100× of K$_d$ for K$_V$1.3) of Cm28 did not inhibit the several other ion channels tested in this study including four other subtypes of K$^+$ channels (K$_V$1.1, K$_V$1.5, K$_V$11.1, K$_{Ca}$1.1, and K$_{Ca}$3.1), two subtypes of Na$^+$ channels (Na$_V$1.5 and Na$_V$1.4), and the voltage-gated H$^+$ channel hH$_V$1. In biological functional studies, Cm28 (at 1.5 μM concentration, ~1,000× of K$_d$ for K$_V$1.3) substantially inhibited the expression of IL2R and CD40L in activated human CD4$^+$ T$_{EM}$ lymphocytes in vitro without compromising cell viability.

Cm28 has a unique primary structure, and it is quite different (Fig. 1 B) from all the other 195 peptide toxins described thus far from scorpion venoms. The closest similarities were found with the ε-KTx family (39–40% identity) and to a less extent with the peptides of α-KTx subfamily 13 (29–33% identity; Fig. 2). In phylogenetic tree analysis, Cm28 and members of ε-KTx family were in the same clade which belongs to α-KTx family (Fig. 3). So far, only two peptide toxins belonging to the ε-KTx family

have been described. They lack a classical secondary structure and exhibit an inhibitor-cystine knot (ICK) type scaffold (Cremonez et al., 2016). In our phylogenetic tree, the ε-KTx family was clade with the α-KTx family; however, its phylogenetic position needs to be confirmed by evaluating a larger number of orthologs to substantiate, at least by phylogenetic analysis, whether the ε-KTx could be a subfamily of the α-KTx with an ICK motif. The branch support values (92 and 80) suggest that Cm28 is completely separated from ε-KTx1.1 and ε-KTx1.2. In addition, the modeled structure of Cm28 shows more similarity to the structure of α-KTx toxins that lack the ICK scaffold. For these reasons, we suggest that Cm28 is the first example of a new subfamily of α-KTxs for which the proposed systematic number is α-KTx 32.1 and its primary sequence has been deposited in Zenodo (Naseem et al., 2022), and will be available in the Uniprot Knowledgebase under accession no. C0HM22. However, a structural study is needed to determine whether Cm28 has an ICK scaffold like the ε-KTxs or whether Cm28 has the characteristic scaffold of the α-KTxs.

The mechanism through which scorpion toxins block K$^+$ channels involve (1) plugging the pore of the channel through binding to the extracellular vestibule (Goldstein and Miller, 1993), and (2) modulating the gating of the channel through binding to the voltage-sensor domain (Swartz and MacKinnon, 1997; Moreels et al., 2017). We argue that Cm28 is not a gating modifier because it did not change the voltage dependence of steady-state activation and the threshold voltage of activation of either K$_V$1.2 or K$_V$1.3 ion channel (Fig. 5, A–E). On the contrary, we propose that Cm28 could be a pore blocker. The blocking
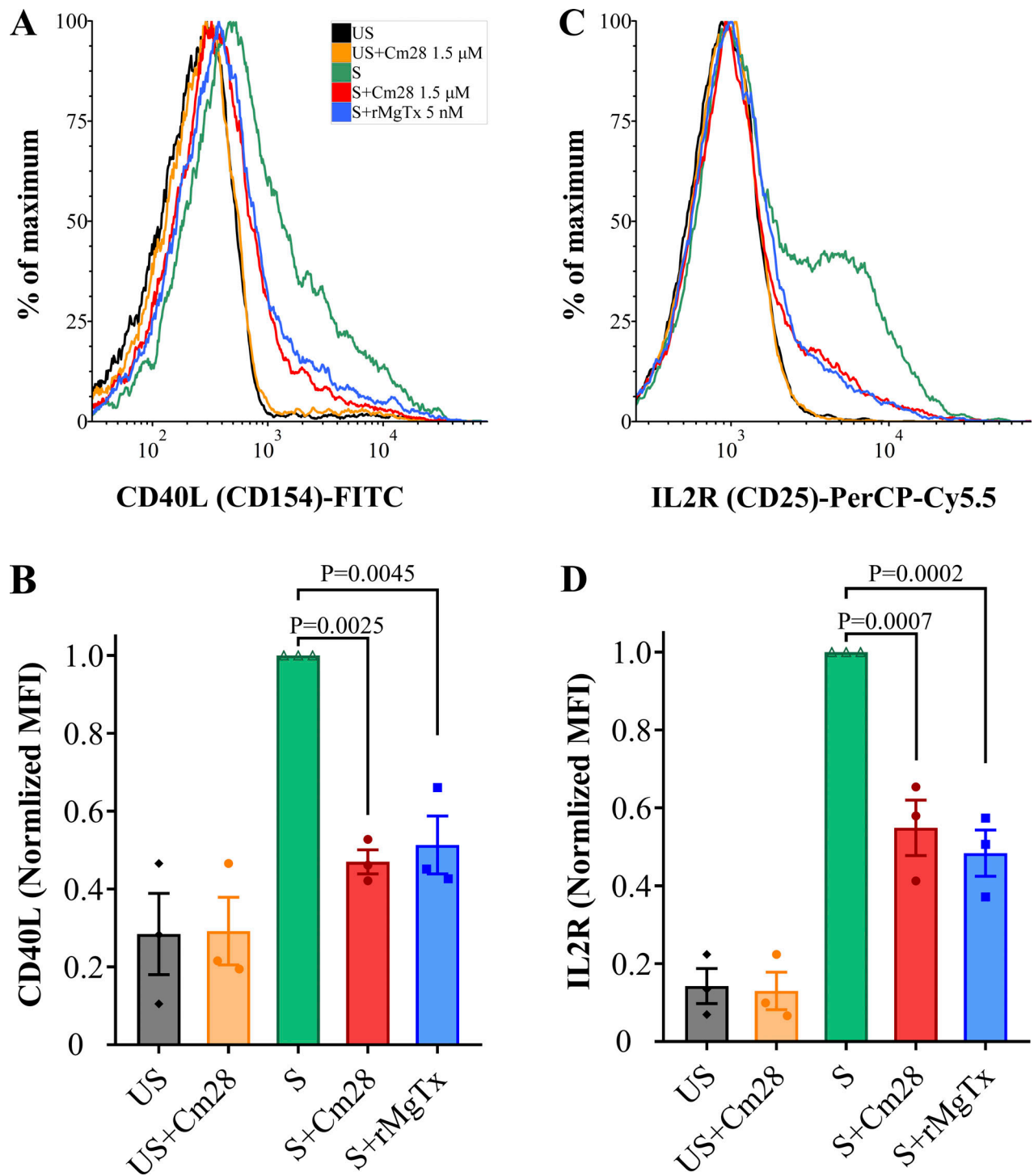
Figure 8. **K$_V$1.3 blockade by Cm28 inhibits the expression of CD40L and IL2R.** Isolated CD4$^+$ T$_{EM}$ lymphocytes were stimulated through TCR with plate-bound anti-human CD3 antibody in the presence or absence of toxins. **(A–D)** After 24 h of stimulation, cells were labeled with anti-CD154 (CD40L; A and B) and anti-CD25 (IL2R) antibodies (C and D). Treatment labels: US, unstimulated (black); US + Cm28, unstimulated in the presence of Cm28 (1.5 μM, orange); S, stimulated with anti-human CD3 antibody coated wells (1 μg/well, green); S + Cm28, stimulated in the presence of Cm28 (1.5 μM, red); S + rMgTx, stimulated in the presence of rMgTx (5 nM, blue). **(A and C)** Fluorescence histograms were obtained from T lymphocytes gated on FSC versus SSC density plot (10,000 events were recorded) and then, peak-normalized overlay histograms were plotted for CD40L and IL2R. A–D follow the same color code. **(B and D)** Mean fluorescence intensities (MFIs) were determined from the histograms and normalized to that of their stimulated but not treated control (S). Bars with individual data points represent values from three independent experiments (two technical repeats in each). Error bars indicate SEM. Statistically significant change in the expression level of CD40L and IL2R is indicated with P values (all pairwise multiple comparison with Tukey's test).

kinetics follows a simple bimolecular interaction between toxin and channel described previously for classical pore blockers such as ChTx (Goldstein and Miller, 1993). The apparent first-order association rate depended on the concentration of Cm28, being faster at higher toxin concentration and the dissociation rate remained constant regardless of change in Cm28 concentration (Fig. 5 F). In addition, the dissociation constants calculated by the k_{off}/k_{on} ratio ($K_d = 1.15$ nM for $K_V1.2$ and $K_d = 2.15$ nM for $K_V1.3$) are very close to the one determined by fitting the Hill equation to the concentration dependence of current inhibition ($K_d = 0.96$ nM for $K_V1.2$ and $K_d = 1.3$ nM for $K_V1.3$). Numerous studies have suggested other mechanisms of block in which a diverse family of toxins target the turret region of K_V channels. The precise molecular processes behind the turret block mechanism remain obscure, however a general concept (turret-block) whereby the toxin acts as a lid above the pore entry was proposed (Saikia et al., 2021). We have recently shown that a turret-modulating toxin may exert its blocking effect by modifying the rates of structural water exchange at the inactivation cavities that are involved in controlling inactivation (Szanto et al., 2021) rather than directly blocking the permeation pathway (Karbat et al., 2019). The turret block mechanism was not addressed in this study as the primary sequence of Cm28 is totally different from Cs1. Cs1 is a low affinity (in the order of micromolar concentrations) and partial blocker of the mammalian K_V channels (Karbat et al., 2019) as opposed to Cm28.

The characteristics of Cm28 block of $K_V1.3$ are consistent with pore blocker toxins; however, in general, pore blocker peptides contain the typical functional dyad or at least the critical lysine residue which protrudes into the selectivity filter of the channel (Goldstein and Miller, 1993). In Cm28, the typical lysine together with an aromatic residue that interacts with the selectivity filter is not found. However, as demonstrated, Cm28 inhibits $K_V1.2$ and $K_V1.3$ with high affinity. There are other small α-KTx peptides (<30 residues long) that show high affinity for $K_V1.3$ channel in the absence of the functional dyad. BmP02 (α-KTx 9.1) and BmP03 (α-KTx 9.2), for example, are toxins that differ by only one amino acid. A Lys at position 16 in BmP02 is replaced by Asn in BmP03. Both toxins inhibit the $K_V1.3$ channel with IC_{50} values of 7 and 85.4 nM, respectively. This 12-fold affinity variation suggests that the Lys16 is a part of the functional surface, even though the typical functional dyad is not found in these toxins (Zhu et al., 2012). Kbot1 toxin (α-KTx 9.5) is 93% identical to BmP02 differing only by two amino acids (N14H and K16V). Nevertheless, Kbot1 is also a potent inhibitor of $K_V1.3$ with an IC_{50} value of 15 nM. It is worth noting that Kbot1, like the BmP03 toxin, does not contain Lys16 but has an IC_{50} closer to that of BmP02, which can be explained by compensating for the loss of cationic charge through the addition of a histidine residue at position 14. Moreover, Kbot1 inhibits the ChTx binding in the rat brain synaptosomes with an IC_{50} of 10 nM (Mahjoubi-Boubaker et al., 2004; Zhu et al., 2012). BmP02, BmP03, and Kbot1 all three belong to the same α-KTx subfamily 9, so it could be that this is a characteristic of this family. However, a short peptide Tt28, from α-KTx 20.1 subfamily lacking the dyad motif, blocks $K_V1.3$ channel with an IC_{50} value of 7.9 nM, although it shares only 25% identity with BmP02

(Abdel-Mottaleb et al., 2006), meaning these short peptides without the functional dyad can be found in other α-KTx subfamilies.

The lack of a functional dyad was also observed for larger peptides (>30 residues in length). By using these toxins as models and applying different approaches, the mechanism underlying the interaction between these peptides and K_V1 channels is revealed. An example is the toxin A24-A33-Pi1, an analog of the toxin Pi1 (α-KTx 6.1). In contrast to the native version, A24-A33-Pi1 lacks the functional dyad K24-Y33. Nevertheless, the toxin was able to bind the channel ($K_d = 22$ μM), indicating that the functional dyad does not appear to be a requirement for recognition and binding to the channel (Mouhat et al., 2004). On the other hand, it has been reported that in the interaction between Tc32 (α-KTX 18.1) and the $K_V1.3$ channel, the differences in the electrostatic properties of the toxin and the channel, the contact surfaces, and the total dipole moment orientations, lead to a lysine residue, even if it located at a different position from the functional dyad, physically blocking the pore of the channel (Stehling et al., 2012). According to the computer simulation, this effect of rearrangement was also observed during the interaction of BmP02 and the $K_V1.3$ channel. After the electrostatic interaction, the side chain of Lys11 was oriented to enter the pore directly, although it has a different structure from the classical dyad motif (Wu et al., 2016). Thus, it could be speculated that the basic residues in Cm28 are involved in the recognition of the channel and the electrostatic forces may rearrange the toxin in such a way that either Lys1 or Lys22 side chain protrude into the pore. Moreover, considering the possibility that another Lys in the toxin takes the place of the canonical lysine of the dyad, it could also be that the dyad is oriented in the opposite way. This phenomenon was previously reported for the toxin κ-KTx1.1, which interacts with the ion channel through a reversed dyad motif, consisting of an aromatic residue Tyr5 and the Lys19 (Srinivasan et al., 2002). In Cm28, the reversed dyad might consist of Tyr13 and Lys22, which could have a similar interaction as the reversed dyad in κ-KTx1.1 toxin. Clearly, extensive structural analysis and molecular docking should be performed to determine whether any of the above mechanisms may be involved in the interaction of Cm28 with $K_V1.1$-$K_V1.3$ channels or whether Cm28 hides an undescribed interaction mechanism.

Several scorpion toxins inhibit $K_V1.3$ with great affinity; however, they also show off-target effects by inhibiting other K^+ channels, thereby compromising their therapeutic potential. For example, HsTX1 (α-KTx-6.3) inhibits $K_V1.1$ in addition to $K_V1.3$ (Lebrun et al., 1997; Regaya et al., 2004) and MgTx (α-KTx-2.2) and ChTx (α-KTx-1.1) blocks more than one $K_V1.x$ channel subtypes with high affinity (Bartok et al., 2014). Vm24 (α-KTx-23.1, previously reported by our group) is the only natural peptide toxin that showed 1,500-fold selectivity for $K_V1.3$ over 10 other ion channels tested (Gurrola et al., 2012; Varga et al., 2012). The selectivity of these attractive peptides could be improved by peptide engineering for therapeutic development. For example, HsTX1[R14A] mutant retained high affinity for $K_V1.3$ and showed 2,000-fold selectivity over $K_V1.1$ (Rashid et al., 2014). An engineered analog of Anuroctoxin (α-KTx-6.12, AnTx) with double substitution (N17A/F32T) was developed previously by

our group which preserved its natural potency for $K_V1.3$, while gaining 16,000-fold selectivity over $K_V1.2$ (Bartok et al., 2015). ShK-186 (originally isolated from sea anemone) is the best example of an engineered analog with high affinity and selectivity for $K_V1.3$ and is under clinical trial for autoimmune diseases called Dalazatide (Pennington et al., 2015; Tarcha et al., 2017). As demonstrated, Cm28 blocks the $K_V1.2$ and $K_V1.3$ with a similar potency (Fig. 4) and shows ~400-fold less affinity for $K_V1.1$ (Fig. 6 A). The order of the blocking potency of Cm28 for various ion channels was $hK_V1.2 \approx hK_V1.3 \gg hK_V1.1 > hK_V1.5 \approx hK11.1 \approx hKCa3.1 \approx mKCa1.1 \approx hNav1.4 \approx hNav1.5 \approx hHv1$ (Fig. 6, B–H). After identifying the key residues in a unique primary structure of Cm28 responsible for interaction with K_V1 channel subtypes, Cm28 peptide can be engineered to improve the selectivity for $K_V1.3$ over $K_V1.1$ and $K_V1.2$.

The potency of Cm28 as a potential immunosuppressor agent was shown in a biological functional assay where the expression of IL2R and CD40L in human $CD4^+$ T_{EM} lymphocytes was determined following TCR-mediated activation. IL2R and CD40L are early, Ca^{2+}-, and NFAT-dependent activation markers of the T_{EM} cells (Schuh et al., 1998; Schonbeck et al., 2000). Since $K_V1.3$ regulates Ca^{2+} signaling, hence the expression level of the IL2R and CD40L, inhibition of $K_V1.3$ leads to a reduced expression level of these early activation markers (Chimote et al., 2017; Veytia-Bucheli et al., 2018; Naseem et al., 2021). Cm28 significantly downregulated the expression of IL2R and CD40L upon TCR-mediated activation of $CD4^+$ T_{EM} cells, similar to the positive control MgTx (Fig. 8), which is consistent with the literature and validates the role of the $K_V1.3$ ion channels in T cell activation through maintaining the Ca^{2+} influx (Panyi et al., 2006; Feske et al., 2015; Veytia-Bucheli et al., 2018). The high concentration of Cm28 (~1,000-fold the K_d for $K_V1.3$) was used in this assay to ensure practically a complete blockade of the $K_V1.3$ channels. Moreover, it was shown that the cell viability after 24 h was not compromised at a high Cm28 concentration (Fig. 7). The use of high toxin concentration is in accordance with the previous reports where significantly higher concentrations of Vm24 and Shk were used in biological assays than the K_d of the toxin for $K_V1.3$ (Beeton et al., 2011; Veytia-Bucheli et al., 2018).

It is worth noting that the path from the discovery of such potential peptides to its therapeutical application requires a variety of steps, most notably the generation of modifications that improve its affinity and selectivity or proteolytic stability, increasing its serum half-life. As mentioned above, there is a wide variety of toxins whose pharmacological targets are potassium channels. However, the size of Cm28 may provide an advantage over other larger peptides that also inhibit $K_V1.2$ or $K_V1.3$ channels. Shorter analogs of ShK toxin have been shown to have lower susceptibility to proteolysis. Reducing the peptide length made the structure of the analogs more constrained, and also reduced the number of positively charged (Lys and Arg) residues and aromatic residues, making the peptides more resistant to degradation by trypsin and chymotrypsin (Krishnarjuna et al., 2018). In addition, other techniques such as peptide cyclization have been used to improve not only proteolytic resistance but also serum stability of short peptides

(González-Castro et al., 2021). Although Cm28 is a promising new peptide, the approaches for increasing the selectivity of Cm28 for $K_V1.3$ discussed above must be utilized and the advantages of the shorter Cm28 over other peptides must be experimentally confirmed to exploit the benefits of Cm28 in the treatment of autoimmune disorders.

References

Abdel-Mottaleb, Y., F.V. Coronas, A.R. de Roodt, L.D. Possani, and J. Tytgat. 2006. A novel toxin from the venom of the scorpion Tityus trivittatus, is the first member of a new α-KTX subfamily. *FEBS Lett.* 580:592–596. https://doi.org/10.1016/j.febslet.2005.12.073

Aiyar, J., J.M. Withka, J.P. Rizzi, D.H. Singleton, G.C. Andrews, W. Lin, J. Boyd, D.C. Hanson, M. Simon, and B. Dethlefs. 1995. Topology of the pore-region of a K^+ channel revealed by the NMR-derived structures of scorpion toxins. *Neuron.* 15:1169–1181. https://doi.org/10.1016/0896 -6273(95)90104-3

Balajthy, A., S. Somodi, Z. Pethő, M. Péter, Z. Varga, G.P. Szabó, G. Paragh, L. Vígh, G. Panyi, and P. Hajdu. 2016. 7DHC-induced changes of Kv1. 3 operation contributes to modified T cell function in Smith-Lemli-Opitz syndrome. *Pflugers Arch.* 468:1403–1418. https://doi.org/10.1007/s00424 -016-1851-4

Bartok, A., K. Fehér, A. Bodor, K. Rákosi, G.K. Tóth, K.E. Kövér, G. Panyi, and Z. Varga. 2015. An engineered scorpion toxin analogue with improved Kv1. 3 selectivity displays reduced conformational flexibility. *Sci. Rep.* 5: 18397. https://doi.org/10.1038/srep18397

Bartok, A., A. Toth, S. Somodi, T.G. Szanto, P. Hajdu, G. Panyi, and Z. Varga. 2014. Margatoxin is a non-selective inhibitor of human Kv1. 3 K^+ channels. *Toxicon.* 87:6–16. https://doi.org/10.1016/j.toxicon.2014.05 .002

Batista, C.V., F. Gómez-Lagunas, R.C. Rodríguez de la Vega, P. Hajdu, G. Panyi, R. Gáspár, and L.D. Possani. 2002. Two novel toxins from the Amazonian scorpion Tityus cambridgei that block Kv1. 3 and Shaker B K⁺-channels with distinctly different affinities. *Biochim.Biophys. Acta*. 1601: 123–131. https://doi.org/10.1016/s1570-9639(02)00458-2

Beeton, C., M. W Pennington, and R. S Norton. 2011. Analogs of the sea anemone potassium channel blocker ShK for the treatment of autoimmune diseases. *Inflamm. Allergy Drug Targets*. 10:313–321. https://doi.org/10.2174/187152811797200641

Beeton, C., H. Wulff, N.E. Standifer, P. Azam, K.M. Mullen, M.W. Pennington, A. Kolski-Andreaco, E. Wei, A. Grino, D.R. Counts, et al. 2006. Kv1. 3 channels are a therapeutic target for T cell-mediated autoimmune diseases. *Proceed. Natl. Acad. Sci. USA*. 103:17414–17419. https://doi.org/10.1073/pnas.0605136103

Beltrán-Vidal, J., E. Carcamo-Noriega, N. Pastor, F. Zamudio-Zuñiga, J.A. Guerrero-Vargas, S. Castaño, L.D. Possani, and R. Restano-Cassulini. 2021. Colombian scorpion *Centruroides margaritatus*: Purification and characterization of a gamma potassium toxin with full-block activity on the hERG1 channel. *Toxins*. 13:407. https://doi.org/10.3390/toxins13060407

Blum, M., H.-Y. Chang, S. Chuguransky, T. Grego, S. Kandasaamy, A. Mitchell, G. Nuka, T. Paysan-Lafosse, M. Qureshi, S. Raj, et al. 2021. The InterPro protein families and domains database: 20 years on. *Nucleic Acids Res.* 49:D344–D354. https://doi.org/10.1093/nar/gkaa977

Buchfink, B., K. Reuter, and H.-G. Drost. 2021. Sensitive protein alignments at tree-of-life scale using DIAMOND. *Nat. Methods*. 18:366–368. https://doi.org/10.1038/s41592-021-01101-x

Cahalan, M.D., and K.G. Chandy. 2009. The functional network of ion channels in T lymphocytes. *Immunol. Rev.* 231:59–87. https://doi.org/10.1111/j.1600-065X.2009.00816.x

Chimote, A.A., P. Hajdu, A.M. Sfyris, B.N. Gleich, T. Wise-Draper, K.A. Casper, and L. Conforti. 2017. Kv1. 3 channels mark functionally competent CD8⁺ tumor-infiltrating lymphocytes in head and neck cancer. *Cancer Res.* 77:53–61. https://doi.org/10.1158/0008-5472.CAN-16-2372

Corzo, G., F. Papp, Z. Varga, O. Barraza, P.G. Espino-Solis, R.C. Rodríguez de la Vega, R. Gaspar, G. Panyi, and L.D. Possani. 2008. A selective blocker of Kv1. 2 and Kv1. 3 potassium channels from the venom of the scorpion Centruroides suffusus suffusus. *Biochem. Pharmacol.* 76:1142–1154. https://doi.org/10.1016/j.bcp.2008.08.018

Cremonez, C.M., M. Maiti, S. Peigneur, J.S. Cassoli, A.A.A. Dutra, E. Waelkens, E. Lescrinier, P. Herdewijn, M.E. De Lima, A.M.C. Pimenta, et al. 2016. Structural and functional elucidation of peptide Ts11 shows evidence of a novel subfamily of scorpion venom toxins. *Toxins*. 8:288. https://doi.org/10.3390/toxins8100288

Dauplais, M., A. Lecoq, J. Song, J. Cotton, N. Jamin, B. Gilquin, C. Roumestand, C. Vita, C.L. de Medeiros, E.G. Rowan, et al. 1997. On the convergent evolution of animal toxins: Conservation of a diad of functional residues in Potassium channel-blocking toxins with unrelated structures. *J. Biol.Chem.* 272:4302–4309. https://doi.org/10.1074/jbc.272.7.4302

Rodríguez de la Vega, R.C., E. Merino, B. Becerril, and L.D. Possani. 2003. Novel interactions between K⁺ channels and scorpion toxins. *Trends Pharmacol. Sci.* 24:222–227. https://doi.org/10.1016/s0165-6147(03)00080-4

Rodríguez de la Vega, R.C., and L.D. Possani. 2004. Current views on scorpion toxins specific for K⁺-channels. *Toxicon*. 43:865–875. https://doi.org/10.1016/j.toxicon.2004.03.022

Eastman, P., J. Swails, J.D. Chodera, R.T. McGibbon, Y. Zhao, K.A. Beauchamp, L.-P. Wang, A.C. Simmonett, M.P. Harrigan, C.D. Stern, et al. 2017. OpenMM 7: Rapid development of high performance algorithms for molecular dynamics. *PLoS Comput. Biol.* 13:e1005659. https://doi.org/10.1371/journal.pcbi.1005659

Feske, S., E.Y. Skolnik, and M. Prakriya. 2012. Ion channels and transporters in lymphocyte function and immunity. *Nat. Rev. Immunol.* 12:532–547. https://doi.org/10.1038/nri3233

Feske, S., H. Wulff, and E.Y. Skolnik. 2015. Ion channels in innate and adaptive immunity. *Annu. Rev. Immunol.* 33:291–353. https://doi.org/10.1146/annurev-immunol-032414-112212

Garcia-Calvo, M., R.J. Leonard, J. Novick, S.P. Stevens, W. Schmalhofer, G.J. Kaczorowski, and M.L. Garcia. 1993. Purification, characterization, and biosynthesis of margatoxin, a component of *Centruroides margaritatus* venom that selectively inhibits voltage-dependent potassium channels. *J. Biol. Chem.* 268:18866–18874. https://doi.org/10.1016/s0021-9258(17)46707-x

Goldstein, S.A., and C. Miller. 1993. Mechanism of charybdotoxin block of a voltage-gated K⁺ channel. *Biophys. J.* 65:1613–1619. https://doi.org/10.1016/S0006-3495(93)81200-1

González-Castro, R., M.A. Gómez-Lim, and F. Plisson. 2021. Cysteine-rich peptides: Hyperstable scaffolds for protein engineering. *ChemBioChem*. 22:961–973. https://doi.org/10.1002/cbic.202000634

Gubič, Š., L.A. Hendrickx, Ž. Toplak, M. Sterle, S. Peigneur, T. Tomašič, L.A. Pardo, J. Tytgat, A. Zega, and L.P. Mašič. 2021. Discovery of Kv1. 3 ion channel inhibitors: Medicinal chemistry approaches and challenges. *Med. Res. Rev.* 41:2423–2473. https://doi.org/10.1002/med.21800

Gurrola, G.B., R.A. Hernández-López, R.C. Rodríguez de la Vega, Z. Varga, C.V.F. Batista, S.P. Salas-Castillo, G. Panyi, F. del Rio-Portilla, and L.D. Possani. 2012. Structure, function, and chemical synthesis of Vaejovis mexicanus peptide 24: A novel potent blocker of Kv1. 3 potassium channels of human T lymphocytes. *Biochemistry*. 51:4049–4061. https://doi.org/10.1021/bi300060n

Hamill, O.P., A. Marty, E. Neher, B. Sakmann, and F.J. Sigworth. 1981. Improved patch-clamp techniques for high-resolution current recording from cells and cell-free membrane patches. *Pflugers Arch.* 391:85–100. https://doi.org/10.1007/BF00656997

Hoang, D.T., O. Chernomor, A. Von Haeseler, B.Q. Minh, and L.S. Vinh. 2018. UFBoot2: Improving the ultrafast bootstrap approximation. *Mol. Biol. Evol.* 35:518–522. https://doi.org/10.1093/molbev/msx281

Hofschröer, V., K. Najder, M. Rugi, R. Bouazzi, M. Cozzolino, A. Arcangeli, G. Panyi, and A. Schwab. 2021. Ion channels orchestrate pancreatic ductal adenocarcinoma progression and therapy. *Front. Pharmacol.* 11:586599. https://doi.org/10.3389/fphar.2020.586599

Jumper, J., R. Evans, A. Pritzel, T. Green, M. Figurnov, O. Ronneberger, K. Tunyasuvunakool, R. Bates, A. Žídek, A. Potapenko, et al. 2021. Highly accurate protein structure prediction with AlphaFold. *Nature*. 596: 583–589. https://doi.org/10.1038/s41586-021-03819-2

Kalyaanamoorthy, S., B.Q. Minh, T.K.F. Wong, A. Von Haeseler, and L.S. Jermiin. 2017. ModelFinder: Fast model selection for accurate phylogenetic estimates. *Nat. Methods*. 14:587–589. https://doi.org/10.1038/nmeth.4285

Karbat, I., H. Altman-Gueta, S. Fine, T. Szanto, S. Hamer-Rogotner, O. Dym, F. Frolow, D. Gordon, G. Panyi, M. Gurevitz, and E Reuveny. 2019. Pore-modulating toxins exploit inherent slow inactivation to block K⁺ channels. *Proc. Natl. Acad. Sci. USA*. 116:18700–18709. https://doi.org/10.1073/pnas.1908903116

Katoh, K., and D.M. Standley. 2013. MAFFT multiple sequence alignment software version 7: Improvements in performance and usability. *Mol. Biol. Evol.* 30:772–780. https://doi.org/10.1093/molbev/mst010

Krishnarjuna, B., C.A. MacRaild, P. Sunanda, R.A.V. Morales, S. Peigneur, J. Macrander, H.H. Yu, M. Daly, S. Raghothama, V. Dhawan, et al. 2018. Structure, folding and stability of a minimal homologue from Anemonia sulcata of the sea anemone potassium channel blocker ShK. *Peptides*. 99: 169–178. https://doi.org/10.1016/j.peptides.2017.10.001

Lam, J., and H. Wulff. 2011. The lymphocyte potassium channels Kv1. 3 and KCa3. 1 as targets for immunosuppression. *Drug Dev. Res.* 72:573–584. https://doi.org/10.1002/ddr.20467

Lebrun, B., R. Romi-Lebrun, M.-F. Martin-Eauclaire, A. Yasuda, M. Ishiguro, Y. Oyama, O. Pongs, and T. Nakajima. 1997. A four-disulphide-bridged toxin, with high affinity towards voltage-gated K⁺ channels, isolated from Heterometrus spinnifer (Scorpionidae) venom. *Biochem. J.* 328: 321–327. https://doi.org/10.1042/bj3280321

Mahjoubi-Boubaker, B., M. Crest, R.B. Khalifa, M. El Ayeb, and R. Kharrat. 2004. Kbot1, a three disulfide bridges toxin from Buthus occitanus tunetanus venom highly active on both SK and Kv channels. *Peptides*. 25: 637–645. https://doi.org/10.1016/j.peptides.2004.02.017

Minh, B.Q., H.A. Schmidt, O. Chernomor, D. Schrempf, M.D. Woodhams, A. Von Haeseler, and R. Lanfear. 2020. IQ-TREE 2: New models and efficient methods for phylogenetic inference in the genomic era. *Mol. Biol. Evol.* 37:1530–1534. https://doi.org/10.1093/molbev/msaa015

Mirdita, M., M. Steinegger, and J. Söding. 2019. MMseqs2 desktop and local web server app for fast, interactive sequence searches. *Bioinformatics*. 35:2856–2858. https://doi.org/10.1093/bioinformatics/bty1057

Mistry, J., S. Chuguransky, L. Williams, M. Qureshi, G.A. Salazar, E.L.L. Sonnhammer, S.C.E. Tosatto, L. Paladin, S. Raj, L.J. Richardson, et al. 2021. Pfam: The protein families database in 2021. *Nucleic Acids Res.* 49: D412–D419. https://doi.org/10.1093/nar/gkaa913

Moreels, L., S. Peigneur, D.T. Galan, E. De Pauw, L. Béress, E. Waelkens, L.A. Pardo, L. Quinton, and J. Tytgat. 2017. APETx4, a novel sea anemone toxin and a modulator of the cancer-relevant potassium channel KV10. 1. *Mar. Drugs*. 15:287. https://doi.org/10.3390/md15090287

Coetzee W.A., Y. Amarillo, J. Chiu, A. Chow, D. Lau, T. McCormack, H. Moreno, M. Nadal, A. Ozaita, D. Pountney, et al. 1999. Molecular

diversity of K⁺ channels. *Ann. NY Acad. Sci.* 868:233–285. https://doi.org/10.1111/j.1749-6632.1999.tb11293.x

Mouhat, S., A. Mosbah, V. Visan, H. Wulff, M. Delepierre, H. Darbon, S. Grissmer, M. De Waard, and J.-M. Sabatier. 2004. The functional dyad of scorpion toxin Pi1 is not itself a prerequisite for toxin binding to the voltage-gated Kv1. 2 potassium channels. *Biochem. J.* 377:25–36. https://doi.org/10.1042/BJ20030115

Naseem, M.U., G. Tajti, A. Gaspar, T.G. Szanto, J. Borrego, and G. Panyi. 2021. Optimization of Pichia pastoris expression system for high-level production of margatoxin. *Front. Pharmacol.* 12:733610. https://doi.org/10.3389/fphar.2021.733610

Naseem, M.U., E. Carcamo-Noriega, J. Beltrán-Vidal, J. Borrego, T.G. Szanto, F.Z. Zamudio, G. Delgado-Prudencio, L.D. Possani, and G. Panyi. 2022. Data file: Amino acid sequence Cm28; a scorpion toxin. *Zenodo.* https://doi.org/10.5281/zenodo.6631118

Ortiz, E., G.B. Gurrola, E.F. Schwartz, and L.D. Possani. 2015. Scorpion venom components as potential candidates for drug development. *Toxicon.* 93:125–135. https://doi.org/10.1016/j.toxicon.2014.11.233

Panyi, G., C. Beeton, and A. Felipe. 2014. Ion channels and anti-cancer immunity. *Philos. Trans. R. Soc. Lond. B Biol. Sci.* 369:20130106. https://doi.org/10.1098/rstb.2013.0106

Panyi, G., L.D. Possani, R.C. Rodríguez de la Vega, R. Gaspar, and Z. Varga. 2006. K⁺ channel blockers: Novel tools to inhibit T cell activation leading to specific immunosuppression. *Current Pharm. Des.* 12:2199–2220. https://doi.org/10.2174/138161206777585120

Papp, F., C.V.F. Batista, Z. Varga, M. Herceg, S.A. Román-González, R. Gaspar, L.D. Possani, and G. Panyi. 2009. Tst26, a novel peptide blocker of Kv1. 2 and Kv1. 3 channels from the venom of Tityus stigmurus. *Toxicon.* 54:379–389. https://doi.org/10.1016/j.toxicon.2009.05.023

Pennington, M.W., S.C. Chang, S. Chauhan, R. Huq, R.B. Tajhya, S. Chhabra, R.S. Norton, and C. Beeton. 2015. Development of highly selective Kv1. 3-blocking peptides based on the sea anemone peptide ShK. *Mar. Drugs.* 13:529–542. https://doi.org/10.3390/md13010529

Peter, M., Jr, Z. Varga, P. Hajdu, R. Gaspar Jr, S. Damjanovich, E. Horjales, L. Possani, and G. Panyi. 2001. Effects of toxins Pi2 and Pi3 on human T lymphocyte Kv1. 3 channels: The role of Glu7 and Lys24. *J. Membr. Biol.* 179:13–25. https://doi.org/10.1007/s002320010033

Rashid, M.H., R. Huq, M.R. Tanner, S. Chhabra, K.K. Khoo, R. Estrada, V. Dhawan, S. Chauhan, M.W. Pennington, C. Beeton, et al. 2014. A potent and Kv1. 3-selective analogue of the scorpion toxin HsTX1 as a potential therapeutic for autoimmune diseases. *Sci. Rep.* 4:4509. https://doi.org/10.1038/srep04509

Regaya, I., C. Beeton, G. Ferrat, N. Andreotti, H. Darbon, M. De Waard, and J.-M. Sabatier. 2004. Evidence for domain-specific recognition of SK and Kv channels by MTX and HsTx1 scorpion toxins. *J. Biol. Chem.* 279:55690–55696. https://doi.org/10.1074/jbc.M410055200

Rezazadeh, S., H.T. Kurata, T.W. Claydon, S.J. Kehl, and D. Fedida. 2007. An activation gating switch in Kv1. 2 is localized to a threonine residue in the S2–S3 linker. *Biophys. J.* 93:4173–4186. https://doi.org/10.1529/biophysj.107.116160

Rokyta, D.R., and M.J. Ward. 2017. Venom-gland transcriptomics and venom proteomics of the black-back scorpion (Hadrurus spadix) reveal detectability challenges and an unexplored realm of animal toxin diversity. *Toxicon.* 128:23–37. https://doi.org/10.1016/j.toxicon.2017.01.014

Saikia, C., O. Dym, H. Altman-Gueta, D. Gordon, E. Reuveny, and I. Karbat. 2021. A molecular lid mechanism of K⁺ channel blocker action revealed by a cone peptide. *J. Mol. Biol.* 433:166957. https://doi.org/10.1016/j.jmb.2021.166957

Sarkar, S., H.M. Nguyen, E. Malovic, J. Luo, M. Langley, B.N. Palanisamy, N. Singh, S. Manne, M. Neal, M. Gabrielle, et al. 2020. Kv1. 3 modulates neuroinflammation and neurodegeneration in Parkinson's disease. *J. Clin. Investig.* 130:4195–4212. https://doi.org/10.1172/JCI136174

Schonbeck, U., F. Mach, and P. Libby. 2000. CD154 (CD40 ligand). *Int. J. Biochem. Cell Biol.* 32:687–693. https://doi.org/10.1016/s1357-2725(00)00016-9

Schuh, K., T. Twardzik, B. Kneitz, J. Heyer, A. Schimpl, and E. Serfling. 1998. The interleukin 2 receptor α chain/CD25 promoter is a target for nuclear factor of activated T cells. *J. Exp. Med.* 188:1369–1373. https://doi.org/10.1084/jem.188.7.1369

Serrano-Albarrás, A., S. Cirera-Rocosa, D. Sastre, I. Estadella, and A. Felipe. 2019. Fighting rheumatoid arthritis: Kv1. 3 as a therapeutic target.

Biochem. Pharmacol. 165:214–220. https://doi.org/10.1016/j.bcp.2019.03.016

Srinivasan, K.N., V. Sivaraja, I. Huys, T. Sasaki, B. Cheng, T.K.S. Kumar, K. Sato, J. Tytgat, C. Yu, B.C.C. San, et al. 2002. κ-Hefutoxin1, a novel toxin from the scorpion heterometrus fulvipes with unique structure and function: Importance of the functional diad in potassium channel selectivity. *J. Biol. Chem.* 277:30040–30047. https://doi.org/10.1074/jbc.M111258200

Stehling, E.G., M.L. Sforça, N.I.T. Zanchin, S. Oyama Jr, A. Pignatelli, O. Belluzzi, E. Polverini, R. Corsini, A. Spisni, and T.A. Pertinhez. 2012. Looking over toxin–K⁺ channel interactions. Clues from the structural and functional characterization of α-KTx toxin Tc32, a Kv1. 3 channel blocker. *Biochemistry.* 51:1885–1894. https://doi.org/10.1021/bi201713z

Swartz, K.J., and R. MacKinnon. 1997. Mapping the receptor site for hanatoxin, a gating modifier of voltage-dependent K⁺ channels. *Neuron.* 18:675–682. https://doi.org/10.1016/s0896-6273(00)80307-4

Szanto, T.G., S. Gaal, I. Karbat, Z. Varga, E. Reuveny, and G. Panyi. 2021. Shaker-IR K⁺ channel gating in heavy water: Role of structural water molecules in inactivation. *J. Gen. Physiol.* 153:e202012742. https://doi.org/10.1085/jgp.202012742

Tabakmakher, V.M., N.A. Krylov, A.I. Kuzmenkov, R.G. Efremov, and A.A. Vassilevski. 2019. Kalium 2.0, a comprehensive database of polypeptide ligands of potassium channels. *Sci. Data.* 6:1–8. https://doi.org/10.1038/s41597-019-0074-x

Tajti, G., D.C.C. Wai, G. Panyi, and R.S. Norton. 2020. The voltage-gated potassium channel KV1. 3 as a therapeutic target for venom-derived peptides. *Biochem. Pharmacol.* 181:114146. https://doi.org/10.1016/j.bcp.2020.114146

Tarcha, E.J., C.M. Olsen, P. Probst, D. Peckham, E.J. Muñoz-Elías, J.G. Kruger, and S.P. Iadonato. 2017. Safety and pharmacodynamics of dalazatide, a Kv1. 3 channel inhibitor, in the treatment of plaque psoriasis: A randomized phase 1b trial. *PLoS One.* 12:e0180762. https://doi.org/10.1371/journal.pone.0180762

Toldi, G., B. Vásárhelyi, A. Kaposi, G. Mészáros, P. Pánczél, N. Hosszufalusi, T. Tulassay, and A. Treszl. 2010. Lymphocyte activation in type 1 diabetes mellitus: The increased significance of Kv1. 3 potassium channels. *Immunol. Lett.* 133:35–41. https://doi.org/10.1016/j.imlet.2010.06.009

Tytgat, J., K.G. Chandy, M.L. Garcia, G.A. Gutman, M.-F. Martin-Eauclaire, J.J. van der Walt, and L.D. Possani. 1999. A unified nomenclature for short-chain peptides isolated from scorpion venoms: α-KTx molecular subfamilies. *Trends Pharmacol. Sci.* 20:444–447. https://doi.org/10.1016/s0165-6147(99)01398-x

Varga, Z., G. Gurrola-Briones, F. Papp, R.C. Rodríguez de la Vega, G. Pedraza-Alva, R.B. Tajhya, R. Gaspar, L. Cardenas, Y. Rosenstein, C. Beeton, et al. 2012. Vm24, a natural immunosuppressive peptide, potently and selectively blocks Kv1. 3 potassium channels of human T cells. *Mol. Pharmacol.* 82:372–382. https://doi.org/10.1124/mol.112.078006

Varga, Z., G. Tajti, and G. Panyi. 2021. The Kv1. 3 K⁺ channel in the immune system and its "precision pharmacology" using peptide toxins. *Biol. Futur.* 72:75–83. https://doi.org/10.1007/s42977-021-00071-7

Veytia-Bucheli, J.I., J.M. Jiménez-Vargas, E.I. Melchy-Pérez, M.A. Sandoval-Hernández, L.D. Possani, and Y. Rosenstein. 2018. Kv1. 3 channel blockade with the Vm24 scorpion toxin attenuates the CD4⁺ effector memory T cell response to TCR stimulation. *Cell Commun. Signal.* 16:45. https://doi.org/10.1186/s12964-018-0257-7

Wang, X., G. Li, J. Guo, Z. Zhang, S. Zhang, Y. Zhu, J. Cheng, L. Yu, Y. Ji, and J. Tao. 2020. Kv1. 3 channel as a key therapeutic target for neuroinflammatory diseases: State of the art and beyond. *Front. Neurosci.* 13:1393. https://doi.org/10.3389/fnins.2019.01393

Wu, B., B.F. Wu, Y.J. Feng, J. Tao, and Y.H. Ji. 2016. Mapping the interaction anatomy of BmP02 on Kv1. 3 channel. *Sci. Rep.* 6:29431. https://doi.org/10.1038/srep29431

Wulff, H., P.A. Calabresi, R. Allie, S. Yun, M. Pennington, C. Beeton, and K.G. Chandy. 2003. The voltage-gated Kv1. 3 K⁺ channel in effector memory T cells as new target for MS. *J. Clin. Investig.* 111:1703–1713. https://doi.org/10.1172/JCI16921

Yang, K.-C., and J.M. Nerbonne. 2016. Mechanisms contributing to myocardial potassium channel diversity, regulation and remodeling. *Trends Cardiovasc. Med.* 26:209–218. https://doi.org/10.1016/j.tcm.2015.07.002

Zhu, L., B. Gao, L. Luo, and S. Zhu. 2012. Two dyad-free Shaker-type K⁺ channel blockers from scorpion venom. *Toxicon.* 59:402–407. https://doi.org/10.1016/j.toxicon.2011.11.016
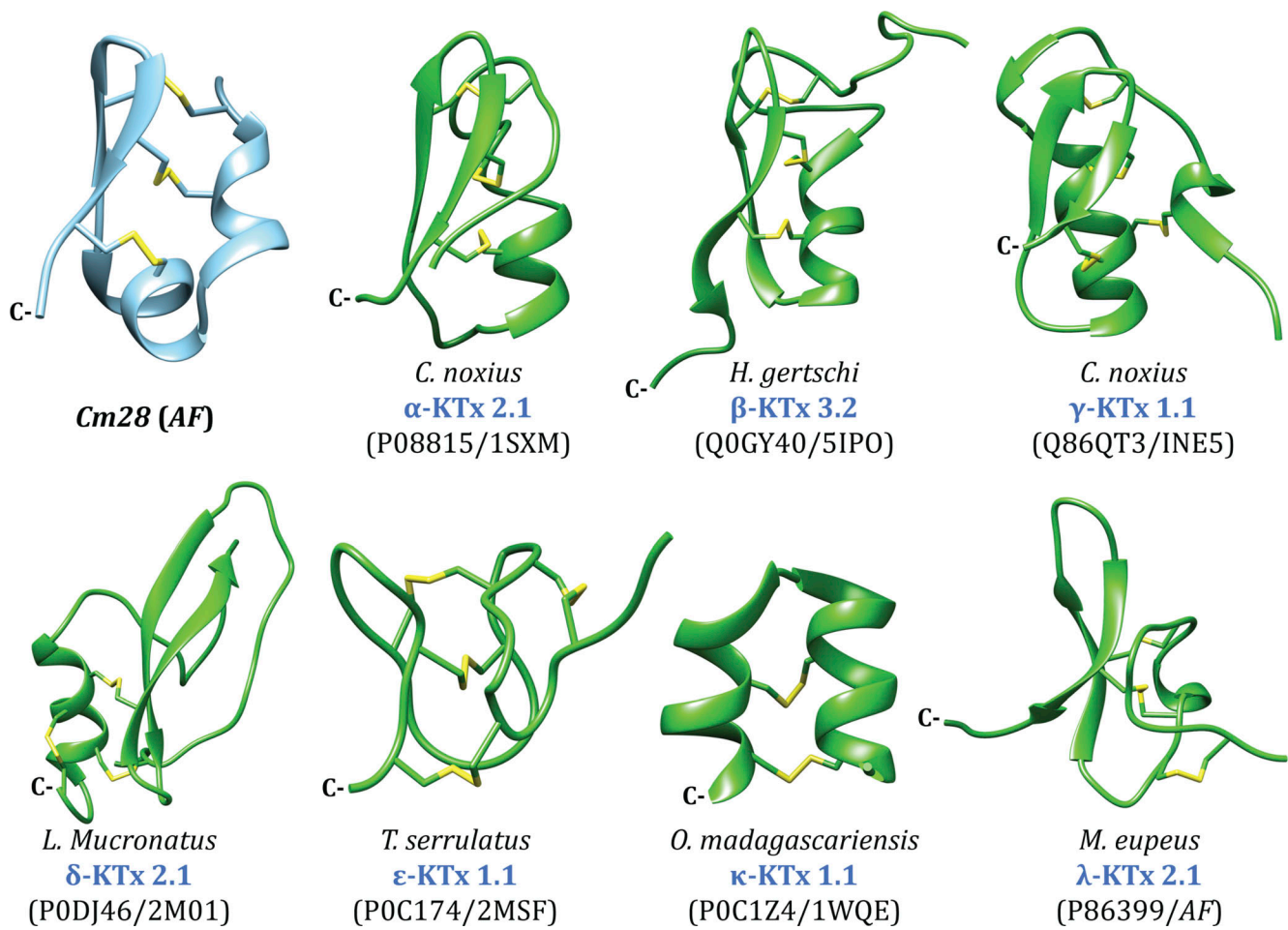
Figure S1. **Comparison of representative 3-D structures of each KTx family with modeled 3-D structure of Cm28.**